

POWER CONTROL OF CDMA-BASED CELLULAR COMMUNICATION
NETWORKS WITH TIME-VARYING STOCHASTIC CHANNEL UNCERTAINTIES

By

SANKRITH SUBRAMANIAN

A THESIS PRESENTED TO THE GRADUATE SCHOOL
OF THE UNIVERSITY OF FLORIDA IN PARTIAL FULFILLMENT
OF THE REQUIREMENTS FOR THE DEGREE OF
MASTER OF SCIENCE

UNIVERSITY OF FLORIDA

2009

© 2009 Sankrith Subramanian

To my parents, P.R. Subramanian and Indhumathi Subramanian; my sister Shilpa;
and my friends and family members, who constantly provided me with motivation,
encouragement and joy

ACKNOWLEDGMENTS

I express my most sincere appreciation to my supervisory committee chair and mentor, Dr. Warren E. Dixon. I thank him for the education, advice, and the encouragement that he had provided me with during the course of my study at the University of Florida. I also thank Dr. John M. Shea for lending his knowledge and support, and providing technical guidance. It is a great privilege to have worked with such far-thinking and inspirational individuals. All that I have learnt and accomplished would not have been possible without their dedication.

I thank all of my colleagues for helping me with my thesis research and creating a friendly work atmosphere. I also extend my appreciation to them, especially Parag M. Patre, Siddhartha S. Mehta, and William Mackunis, for sharing their knowledge and encouraging some thought-provoking analytical discussions.

Most importantly, I would like to express my deepest appreciation to my parents P. R. Subramanian and Indhumathi Subramanian and my sister Shilpa. Their love, understanding, patience and personal sacrifice made this dissertation possible.

TABLE OF CONTENTS

	<u>page</u>
ACKNOWLEDGMENTS	4
LIST OF TABLES	7
LIST OF FIGURES	8
ABSTRACT	9
CHAPTER	
1 INTRODUCTION	10
2 Radio-Channel Modeling	14
3 Robust Power Control of Cellular Communication Networks with Time-Varying Channel Uncertainties	22
3.1 Control Development	22
3.1.1 Control Objective	22
3.1.2 Closed-Loop Error System	23
3.2 Stability Analysis	24
3.3 Estimation of Error at Unsamped Instances	25
3.4 Simulation	28
3.4.1 Network Mobility Model	28
3.4.2 Simulation Results	32
4 Prediction-Based Power Control of Distributed Cellular Communication Networks with Time-Varying Channel Uncertainties	35
4.1 Network Model	36
4.2 Linear Prediction of Fading Coefficient	37
4.3 Control Development	40
4.3.1 Control Objective	40
4.3.2 Closed Loop Error System	41
4.4 Stability Analysis	43
4.5 Simulation Results	45
5 CONCLUSION	51
5.1 Summary of Results	51
5.2 Recommendations for Future Work	52
APPENDIX	
A ESTIMATION OF RANDOM PROCESSES	53

A-1	General MMSE based estimation theory	53
A-2	Gaussian Case	54
B	Orthogonality Condition	56
	REFERENCES	58
	BIOGRAPHICAL SKETCH	61

LIST OF TABLES

<u>Table</u>		<u>page</u>
3-1	Percentage of samples within the desired SINR range	33
4-1	Percentage of samples within the desired SINR range	49

LIST OF FIGURES

<u>Figure</u>	<u>page</u>
2-1 Reverse link.	15
2-2 Fading due to Doppler shift and scattering.	15
2-3 Probability density function (PDF) of a Rayleigh random variable.	17
2-4 Power of the received envelope for a 10Hz fading channel.	18
3-1 Autocorrelation function for fading.	28
3-2 Cellular network topology - random way-point mobility model	29
3-3 Error plot: MTs with low doppler frequencies.	30
3-4 Error plot: MTs with high doppler frequencies.	31
3-5 Error, channel gain and power plot: MT with a doppler frequency of 1.98 Hz.	31
3-6 Error, channel gain and power plot: MT with a doppler frequency of 34.14 Hz.	32
4-1 Distributed cellular network topology.	45
4-2 Error, channel gain, and power plot of a MT with maximum Doppler frequency 4.11 Hz.	46
4-3 Prediction error of the MT with maximum Doppler frequency 4.11 Hz.	47
4-4 Error, channel gain, and power plot of a MT with maximum Doppler frequency 30.9 Hz.	47
4-5 Prediction error of the MT with maximum Doppler frequency 30.9 Hz.	48
4-6 Comparison of high gain and predictive power control algorithms.	50

Abstract of Thesis Presented to the Graduate School
of the University of Florida in Partial Fulfillment of the
Requirements for the Degree of Master of Science

POWER CONTROL OF CDMA-BASED CELLULAR COMMUNICATION
NETWORKS WITH TIME-VARYING STOCHASTIC CHANNEL UNCERTAINTIES

By

Sankrith Subramanian

May 2009

Chair: Warren E. Dixon

Co-Chair: John M. Shea

Major: Electrical and Computer Engineering

Power control is used to ensure that each link achieves its target signal-to-interference-plus-noise ratio (SINR) to effect communication in the reverse link (uplink) of a wireless cellular communication network. In cellular systems using direct-sequence code-division multiple access (CDMA), the SINR depends inversely on the power assigned to the other users in the system, creating a nonlinear control problem. Due to the spreading of bands in CDMA based cellular communication networks, the interference in the system is mitigated. The nonlinearity now arises by the uncertain random phenomena across the radio link, causing detrimental effects to the signal power that is desired at the base station. Mobility of the terminals, along with associated random shadowing and multi-path fading present in the radio link, results in uncertainty in the channel parameters. To quantify these effects, a nonlinear MIMO discrete differential equation is built with the SINR of the radio-link as the state to analyze the behavior of the network. Controllers are designed based on analysis of this networked system, and power updates are obtained from the control law. Analysis is also provided to examine how mobility and the desired SINR regulation range affects the choice of channel update times. Realistic wireless network mobility models are used for simulation and the power control algorithm formulated from the control development is verified on this mobility model for acceptable communication.

CHAPTER 1 INTRODUCTION

Various transmitter power control methods have been developed to deliver a desired quality of service (QoS) in wireless networks [1–8]. Early work on power control using a centralized approach was investigated in [9] and [10]. The concept of Signal-to-Interference (SIR) balancing was introduced in [9] and [10], where all receivers experience the same SIR levels. Maximum achievable SIRs were formulated considering the SIR balancing problem as an eigenvalue problem. A stochastic distributed transmitter power approach was also investigated in [6–8]. Methods were developed to reduce co-channel interference for a given channel allocation using transmitter power control in [6] and [8]. In [6], transmitter power control schemes are developed to reduce the cochannel interferences, the performance of which is measured by defining Outage probabilities as the probability of having a too low Signal to Interference (SIR) ratio. An optimum (in the sense that the outage or interference probability is minimized) eigenvalue based power control scheme is employed using this approach.

The performance of optimum transmitter power control algorithms is investigated in [8]. Performance bounds and conditions of stability for all types for transmitter power control algorithms are found. The system model is developed using N cells with M independent channel pairs (and hence crosstalk between channels is neglected). The thermal noise is neglected, as an interference limited system is considered. A link gain matrix is introduced in [8], each of the components is defined as the link gain from the base station in cell j to the mobile terminal in cell i , normalized to the link gain in the desired path, from base station i to mobile terminal i . In [8], a global power control algorithm is defined as an algorithm that has access to the entire gain matrix in every instant. An optimum power control algorithm that minimizes the interference probability is proposed in [8] assuming global power control, and the performance bounds are derived

for this algorithm. A Stepwise Removal Algorithm (SRA) is proposed in [8] that minimizes the computational requirements, suffered by the optimal power control algorithm.

To address the problems associated with measurements of link gains in [8], a distributed approach was made in [7], where only SIR measurements in those links actually in use are made. A distributed SIR balancing scheme is developed and a discrete time power control algorithm (DPCA) is proposed as

$$P(l + 1) = \beta ZP(l), \quad (1-1)$$

where P is the power vector, and β is a control gain chosen to avoid increasing powers. Due to the difficulty in calculating this quantity, a stepwise removal with distributed balancing scheme is developed in [7]. These algorithms were framed when only path loss was effecting the channel uncertainty.

A centralized SIR balancing power control scheme was formulated in [11]. Fading and noise were ignored in this approach. An eigenvalue approach aimed at achieving the same target SIR for all the radio links is used. An upper limit for the power was imposed to each user in the constrained power control algorithm of [3], and an optimum power control for maximizing the minimum SIR is formulated.

A simple distributed autonomous power control algorithm was introduced in [2] where channel reuse is maximized. Networks where certain power settings exists are considered and exponential fast convergence to such settings is demonstrated in [2]. Local measurements were made in [2] to meet the target SINR in each channel. For this purpose, the distributed control law is manipulated in terms of the power, and SINR for mobile terminal in a radio link. Making local measurements helps in [2] implies that the SINR for each radio channel at every sampling instant is measurable, the SINR being a function of not only a interference in the current cell, but also co-channel interferences from adjacent cells. Based on the linear analysis of the system, and constraining the eigenvalues, the power approaches an optimal power vector. The power algorithm formulation for this

approach is applicable to both uplink (mobile terminal to base station) and downlink (base station to mobile terminal) channels.

A framework which integrates power control and base station assignment was introduced by [12]. A Minimum Transmitted Power (MTP) was formulated for a CDMA-based system in which the total power is minimized subject to maintaining an individual target SIR for each mobile. Synchronous (power updates are done at the same sampling rate for all radio links) and asynchronous (power updates done at different sampling rates for different radio links) distributed algorithms that find the optimal power vector and base station assignment is identified.

A generalized framework for uplink iterative power control is provided in [5], where common properties for interference constraints are identified. The problem of finding the power control vector for the radio links to achieve acceptable communication is reduced to satisfying a vector inequality condition stated in [5] as the interference that a user must overcome to achieve an acceptable connection. Synchronous and asynchronous power control converge to an optimal power which minimizes the total transmitted power.

Active link protection (ALP) schemes were introduced in [1] and [13], where the QoS of active links is maintained above a threshold limit to protect the link quality. In [1], the Foschini-Miljanic power control algorithm is modified for reduced measurements and emphasis was given on ALP for Distributed Power Control (DPC).

Optimal power control algorithm with outage-probability constraints was developed in [14], where the network is interference-limited with Rayleigh fading of both the desired and interference signals. Power control with joint Multiuser Detection (MUD) scheme was developed in [15] for Rayleigh faded systems with outage constraints.

Recently, a distributed power control scheme was suggested in [16] in the presence of radio channel uncertainties caused by mobility of the user terminals. These channel uncertainties include exponential path loss, shadowing, and multi-path fading, which are modeled as random variables in the SINR measurements. The uncertainty of the

multi-path fading effects provided motivation for the results in [16] and [17]. Specifically, a persistently exciting adaptation scheme is proposed in [16] and [17]. However, in these works, the fading process is modeled as slowly changing so that the channel gain can be accurately estimated and practical limitations of transmission power limitations are not considered.

Of the channel uncertainties, multi-path fading has the most critical effect on the design of a power-control system because of the time and amplitude scales. Multi-path fading is caused by reflections in the environment, which cause multiple time-delayed versions of the transmitted signal to add together at the receiver. The time offsets cause the signals to add with different phases, and thus multi-path fading can change significantly over distance scales as short as a fraction of a wavelength. For instance, for a system using the 900 MHz cellular band, the channel coherence time (the time for which the channel is essentially invariant) for a mobile terminal traveling at 30 miles/hour is approximately 10 ms. There is a need to quantify the multi-path fading effects of the channel in the system. In this thesis, efforts are made to understand the fading phenomena in the radio channel of a CDMA-based cellular communication network and quantify them to develop power control algorithms. The modeling of cellular communication networks is based on analysis of the nonlinear networked system and Lyapunov-based control structures are formulated for such systems in this thesis. An analytical approach to choosing power update sampling time is used in this thesis where channel uncertainties (especially Rayleigh fading) are quantified based on estimation of error between the desired and actual Signal-to-Interference plus Noise Ratio (SINR).

CHAPTER 2 RADIO-CHANNEL MODELING

In this chapter, the characteristics of the reverse link of the radio channel is investigated and modeled.

The channel gain of a radio link (see Figure 2-1) is comprised of three components: Exponential path-loss, Log-normal shadowing, and Multi-path fading. The gain of the channel is defined [18] as

$$g_{ii}(l) = g_{d_0} \left(\frac{d_i(l)}{d_0} \right)^{-\kappa} 10^{0.1\delta_i(l)} |X_i(l)|^2, \quad (2-1)$$

where the term $|X_i(l)|^2$ is used to model Rayleigh fading., g_{d_0} is the near-field gain given by [19]

$$g_{d_0} = \frac{G_t G_r \lambda^2}{(4\pi)^2 d_0^2 L}, \quad d_f \leq d_0 \leq d_i(l), \quad (2-2)$$

where G_t is the transmitter antenna gain, G_r is the receiver antenna gain, λ is the wavelength in meters, L is the system-loss factor, d_0 is the distance between the transmitter and receiver antenna, and $d_f = 6m$ is the Fraunhofer distance. Without loss of generality, G_t , G_r , and L are all assumed to be 1. Since the power updates are provided at discrete instances due to bandwidth constraints, the system is analyzed at discrete instances of time ($l \in \mathbb{Z}$). For this reason, the continuous time channel parameters are analyzed and a suitable channel sampling time is chosen in Chapter 3.

The term $\left(\frac{d_i(l)}{d_0} \right)^{-\kappa}$ is used to model the average path loss at distance $d_i(l)$ from mobile terminal (MT) i to the base station (BS), where κ is the path-loss exponent, which typically takes values between two and five. The term $10^{0.1\delta_i(l)}$ is used to model large-scale log-normal shadowing from buildings, terrain, or foliage, where $\delta_i(l)$ is a Gaussian random process (see [19]).

Figure 2-2 shows the typical scenario of a MT communicating with a BS. The received signal at the BS is faded due to the mobility of the MTs causing doppler shifts in the frequency of the received wave and multipath propagation of the wave caused

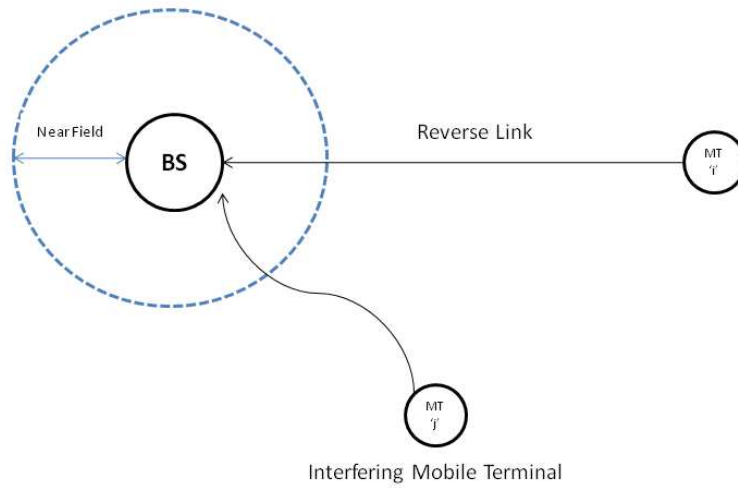


Figure 2-1. Reverse link.

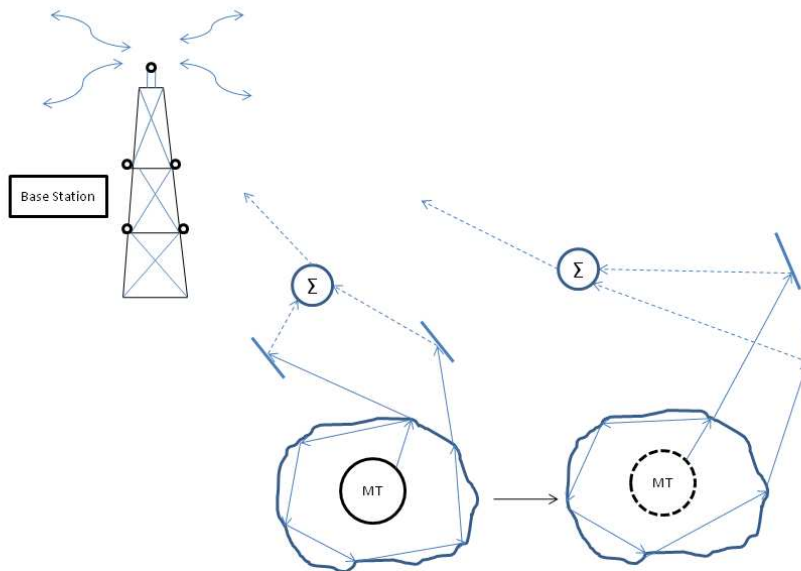


Figure 2-2. Fading due to Doppler shift and scattering.

by scattering in the presence of surrounding objects. These individual components add up in a constructive or destructive manner, depending on random phase shifts of these components of the received signal.

The received fading component of the signal can be represented as [19]

$$X_i(t) = G_c(t) \cos(2\pi f_c t) - G_s(t) \sin(2\pi f_c t) \quad (2-3)$$

where f_c is the carrier frequency, the Gaussian random processes $G_c(t)$ and $G_s(t)$ are defined as

$$G_c(t) = E_0 \sum_{n=1}^N C_n \cos(2\pi f_n t + \phi_n) \quad (2-4)$$

$$G_s(t) = E_0 \sum_{n=1}^N C_n \sin(2\pi f_n t + \phi_n). \quad (2-5)$$

The processes $G_c(t)$ and $G_s(t)$ are uncorrelated zero-mean Gaussian random variables for any t with equal variance $\frac{E_0^2}{2}$, where E_0 is the real amplitude of the local average E-field (assumed constant), C_n is the real random variable representing the amplitude of individual waves, ϕ_n is the phase shift due to reflections of the individual waves and is a uniform random variable in $[0, 2\pi]$, N is the number of scattered waves, and $f_n(t)$ is the doppler frequency defined as

$$f_n = \frac{v}{\lambda} \cos \theta. \quad (2-6)$$

In Equation 2-6, $v(t)$ is the velocity of motion of the MT and $\theta(t)$ is the angle between the transmitted signal and the direction of motion of the MT.

The envelope of the received signal (E-field) is

$$|X_i(t)| = \sqrt{G_c^2(t) + G_s^2(t)}, \quad (2-7)$$

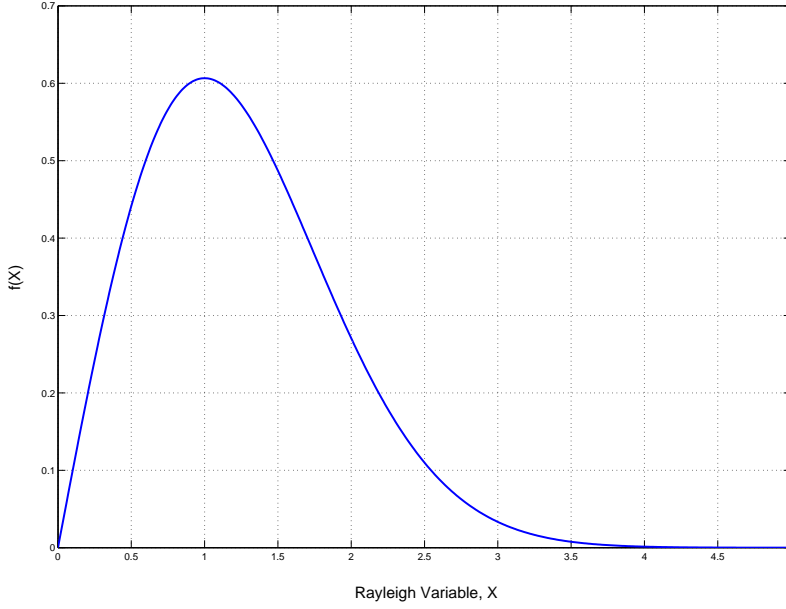


Figure 2-3. Probability density function (PDF) of a Rayleigh random variable.

where $|X_i(t)|$ is a random variable with a Rayleigh distribution with a probability density function of (refer to Figure 2-3)

$$\begin{aligned}
 p(|X_i|) &= \frac{X_i}{\left(\frac{E_0^2}{2}\right)} \exp\left(-\frac{X_i^2}{2\left(\frac{E_0^2}{2}\right)}\right), & 0 \leq X_i \leq \infty \\
 &= 0, & X_i < 0.
 \end{aligned} \tag{2-8}$$

Squaring Equation 2-7 yields the fading power, i.e.,

$$|X_i(t)|^2 = G_c^2(t) + G_s^2(t). \tag{2-9}$$

The power of the received envelope for a faded radio channel (Doppler frequency = 10Hz) is shown in Figure 2-4.

For analytical purposes, $X_i(t)$ is usually taken to be a complex-valued Gaussian random process, and thus $|X(t)|$ is a Rayleigh random variable for each t when $E[X(t)] = 0$ (the operator $E[X]$ is used to represent the expected value of a random variable X), which corresponds to no line-of-sight path from the MT to the BS. Gaussian random

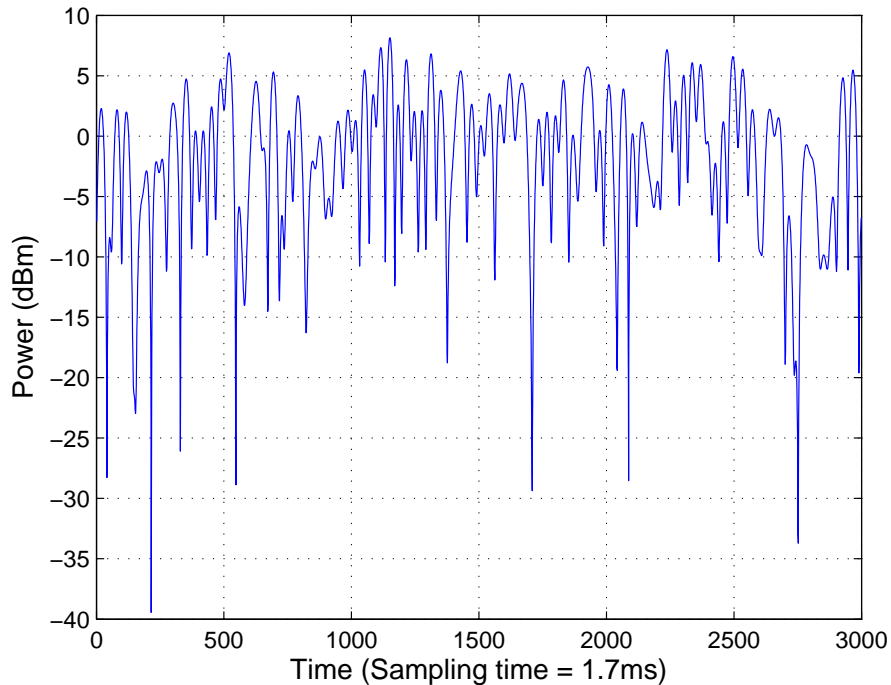


Figure 2-4. Power of the received envelope for a 10Hz fading channel.

processes provide good models for the log-normal shadowing and Rayleigh fading over the most-probable range of reception. However, both of these processes are unbounded, which means that any received power level is possible. However, $g_{ii}(l)$ cannot take arbitrarily large values in practice because the received power cannot exceed the transmitted power. Furthermore, a cellular system cannot practically transmit to *overfaded* users who are in very deep fades (i.e., when $g_{ii}(l)$ is close to zero) because doing so would require extremely large power at that user and the other users (because the power transmitted to each user causes interference at the other users) [20]. Hence, the subsequent development is based on the assumption that the fading power $|X_i(\cdot)|^2$ is bounded and non-zero.

The development in this thesis considers the reverse channel (from the MTs to the BS) and investigates control of the SINRs for the MTs. The SINR at MT i , denoted by $x_i(l) \in \mathbb{R}$, can be expressed as [21]

$$x_i(l) = \frac{ag_{ii}(l)P_i(l)}{I_i(l)}, \quad (2-10)$$

where $P_i(l) \in \mathbb{R}$ is the power from the MT i to the BS, and $g_{ii}(l) \in \mathbb{R}$ is the channel gain from the BS to the MT i . In Equation 2-10, $I_i(l) \in \mathbb{R}$ denotes the interference-plus-noise power at the BS due to transmissions by other MTs in the cellular network, defined as

$$I_i(l) = \sum_{j \neq i} g_{ij}(l)P_j(l) + a\eta_i, \quad (2-11)$$

where $g_{ij}(l) \in \mathbb{R}$ is the channel gain for the link between MT j and the BS that affects the interference in the radio link between MT i and the BS, $P_j(l) \in \mathbb{R}$ is the power transmitted by MT j to the BS, and $\eta_i \in \mathbb{R}$ denotes the thermal noise in link i . In a CDMA based network, each radio link is forced to share the same bandwidth; hence, $I_i(\cdot)$ is non-zero and bounded. The bandwidth spreading factor, or the processing gain [22] for the cellular system using CDMA is denoted by a defined as

$$a = \frac{W}{R}, \quad (2-12)$$

where W is the transmission bandwidth, in hertz, and R is the data rate in bits/second. By increasing the bandwidth spreading factor, the interference of the system can be reduced. Therefore, focus is laid on the effects of fading in the radio channel in this thesis to develop power controllers for radio links operating in a CDMA based cellular communication network.

The first difference of the SINR defined in Equation 2-10 can be determined as

$$\begin{aligned} \Delta x_i(l) &= a (I_i(l) + \Delta I_i(l))^{-1} \left(\frac{\Delta g_{ii}(l)}{T_s} \right) P_i(l) + a (I_i(l) + \Delta I_i(l))^{-1} g_{ii}(l) \left(\frac{\Delta P_i(l)}{T_s} \right) \\ &\quad - \{I_i(l) (I_i(l) + \Delta I_i(l))\}^{-1} \left\{ a \left(\sum_{i \neq j} \left(\frac{\Delta g_{ij}(l)P_j(l)}{T_s} \right) \right) g_{ii}(l)P_i(l) \right. \\ &\quad \left. + a \left(\sum_{i \neq j} \left(\frac{g_{ij}(l)\Delta P_j(l)}{T_s} \right) \right) g_{ii}(l)P_i(l) \right\} + [\{a (I_i(l) + \Delta I_i(l))\}^{-1} \\ &\quad \cdot \left(\frac{\Delta g_{ii}(l)}{T_s} \right) \left(\frac{\Delta P_i(l)}{T_s} \right) \left. \right\} - a \sum_{i \neq j} \left(\frac{\Delta g_{ij}(l)\Delta P_j(l)}{T_s^2} \right) \\ &\quad \cdot \{I_i(l) (I_i(l) + \Delta I_i(l))\}^{-1} g_{ii}(l)P_i(l) \end{aligned} \quad (2-13)$$

where Equation 2–10 and Equation 2–11 were used, and T_s is the power update interval. Neglecting the residual terms in square brackets in Equation 2–13, approximating $(I_i(l) + \Delta I_i(l)) \approx I_i(l)$, and using Equation 2–10 yields

$$x_i(l+1) = \alpha_i(l, x)x_i(l) + u_i(l), \quad (2-14)$$

where $\alpha_i(l, x) \in \mathbb{R}$ is an unknown, time-varying state-dependent quantity, defined as

$$\begin{aligned} \alpha_i(l, x) &= ag_{ii}(l+1)g_{ii}^{-1}(l) - a \left(\sum_{i \neq j} (\Delta g_{ij}(l)P_j(l)) \right) I_i^{-1}(l) - a \left(\sum_{i \neq j} (g_{ij}(l)\Delta P_j(l)) \right) I_i^{-1}(l) \\ \implies \alpha_i(l, x) &= aI_i^{-1}(l)P_i(l) \left[\frac{g_{ii}(l+1)}{x_i(l)} - \sum_{i \neq j} \frac{(\Delta g_{ij}(l)P_j(l))}{P_i(l)} + \sum_{i \neq j} \frac{(g_{ij}(l)\Delta P_j(l))}{P_i(l)} \right], \end{aligned} \quad (2-15)$$

and $u_i(l) \in \mathbb{R}$ is the control input, defined as

$$u_i(l) = \frac{x_i(l)}{P_i(l)} [P_i(l+1) - P_i(l)], \quad (2-16)$$

since

$$\frac{ag_{ii}(l)}{I_i(l)} = \frac{x_i(l)}{P_i(l)}.$$

After including measurement noise $\xi_i(l, x)$, the expression in Equation 2–14 can be rewritten as

$$x_i(l+1) = \alpha_i(l, x)x_i(l) + u_i(l) + \xi_i(l, x). \quad (2-17)$$

By defining the interference $I(l) \in \mathbb{R}^{n \times n}$ as a diagonal matrix with entries $I_i(l)$ expressed in Equation 2–11, $g(l) \in \mathbb{R}^{n \times n}$ as a diagonal matrix with entries $g_{ii}(l)$, and $P(l) \in \mathbb{R}^n$, then the MIMO system can be developed as

$$x(l+1) = \alpha(l, x)x(l) + u(l) + \xi(l, x), \quad (2-18)$$

where $\alpha(l, x) = \text{diag}(\alpha_i(l, x)) \in \mathbb{R}^{n \times n}$ denotes the unknown, time-varying state-dependent diagonal matrix (since $\alpha_i(l, x)$ is a function of the state $x_i(l)$ as shown in the Equation 2–15) which can be assumed to be upper bounded by a known positive constant from the preceding discussion on the uncertain channel parameters, $x(l) \in \mathbb{R}^n$ is the state vector at

instant l , $u(l) \in \mathbb{R}^n$ is the control input vector, $x(l+1) \in \mathbb{R}^n$ is the state vector at instant $l+1$, and $\xi(l, x) \in \mathbb{R}^n$ is the stochastic measurement noise bounded by a known constant. The measurement noise is assumed to be bounded by a positive constant.

Here, $u(l)$ is expressed in terms of the power update law as

$$P_i(l+1) = \frac{u_i(l)}{x_i(l)} P_i(l) + P_i(l). \quad (2-19)$$

CHAPTER 3
ROBUST POWER CONTROL OF CELLULAR COMMUNICATION NETWORKS
WITH TIME-VARYING CHANNEL UNCERTAINTIES

In this chapter, the objective is to design and analyze the performance of a controller for use in a radio channel operating in a CDMA based cellular communication network with Rayleigh fading following Clarke's model [23]. The Rayleigh fading process produces unbounded changes in the SINRs with non-zero probability, even for arbitrarily short time scales, but by using the concept of overfaded users [20], the channel gains can be bounded. Based on this model, a simple proportional controller to minimize the sampled SINR error is developed in this chapter. Specifically, despite uncertainty in the multi-path fading effects, a Lyapunov-based analysis is used to develop an ultimate bound for the sampled SINR error which is a function of the upper bound on the channel uncertainty divided by a nonlinear damping gain that can be made arbitrarily large up to some upper value dictated by the power update law. The performance of this controller is evaluated in this chapter via simulation under realistic power limits and channel changes based on the standard random-waypoint mobility model. A statistical analysis of the performance effects of fading between the sampling intervals is considered in this chapter, which is used to discuss the choice of the control update rate. Additional analysis is provided to conclude that the expected value of the squared norm of the SINR error converges to an ultimate bound that is a function of sampling rate. Therefore, the sampling rate can be adjusted to keep the SINR error within a desired range that allows for signal decoding. Simulation results are provided for a Random-Waypoint model that illustrates the performance of the developed controller.

3.1 Control Development

3.1.1 Control Objective

The SINR should remain between two thresholds as

$$\gamma_{\min} \leq x_i \leq \gamma_{\max} \tag{3-1}$$

to achieve acceptable communication performance over the link while minimizing interference to adjacent cells. The control objective for the following development is to regulate the SINR to a target value for each channel, denoted by $\gamma \in \mathbb{R}^n$, while ensuring that the SINR remains between the specified lower and upper limits for each channel, as described in Equation 3-1. To quantify the objective, a regulation error $e(l) \in \mathbb{R}^n$ is defined as

$$e(l) = x(l) - \gamma. \quad (3-2)$$

3.1.2 Closed-Loop Error System

The first difference of the regulation error, denoted as $\Delta e(l) \in \mathbb{R}^n$, is

$$\begin{aligned} \Delta e(l) &= e(l+1) - e(l) = x(l+1) - x(l) \\ &= \alpha(l, x)x(l) + u(l) + \xi(l, x) - x(l). \end{aligned} \quad (3-3)$$

To facilitate the subsequent analysis, the expression in Equation 3-3 is rewritten as

$$\Delta e(l) = \chi(l, x) + \Omega(l, x) + u(l), \quad (3-4)$$

where $\chi(l, x) \in \mathbb{R}^n$ denotes an auxiliary term defined as

$$\chi(l, x) = (\alpha(l, x) - I^{n \times 1}) e(l), \quad (3-5)$$

and $\Omega(l, x) \in \mathbb{R}^n$ is defined as

$$\Omega(l, x) = (\alpha(l, x) - I^{n \times 1}) \gamma + \xi(l, x). \quad (3-6)$$

Motivation for introducing the auxiliary terms in Equation 3-5 and Equation 3-6 is to collect terms that have a common upper bound. Specifically, upper bounds for $\chi(l, x)$ and $\Omega(l, x)$ can be developed as

$$\|\chi(l, x)\| \leq c_1 \|e(l)\| \text{ and } \|\Omega(l, x)\| \leq c_2, \quad (3-7)$$

where $c_1, c_2 \in \mathbb{R}$ denote known positive constants. Based on Equation 3-4, Equation 3-7, and the subsequent stability analysis, a proportional controller is designed as

$$u(l) \triangleq -(c_1 + k_n + k_1) e(l), \quad (3-8)$$

where c_1 is introduced in Equation 3-7, and $k_1, k_n \in \mathbb{R}$ denote positive control gains.

Based on Equation 2-19 and Equation 3-8, the power update law is

$$P_i(l+1) = \frac{-(c_1 + k_n + k_1) e_i(l) P_i(l)}{(e_i(l) + \gamma)} + P_i(l) \quad (3-9)$$

under the constraint that $0 < P_i(l) \leq P_{\max}$, where P_{\max} is a maximum power level. After substituting Equation 3-8 into Equation 3-4, the closed-loop error system for $e(l)$ can be determined as

$$\Delta e(l) = \chi(l, x) + \Omega(l, x) - (c_1 + k_n + k_1) e(l).$$

3.2 Stability Analysis

Theorem 3-1: The controller in Equation 3-8 and Equation 3-9 ensures that the SINR regulation error approaches an ultimate bound $\varepsilon(k_n, l_0) \in \mathbb{R}$ in the sense that

$$\|e(l)\| \rightarrow \varepsilon(k_n, l_0) \text{ as } l \rightarrow \infty. \quad (3-10)$$

Proof: Let $V(e, l) : D \times [0, \infty) \rightarrow \mathbb{R}$ be a positive definite function defined as

$$V(e, l) = \frac{1}{2} e^T(l) e(l). \quad (3-11)$$

After taking the first difference of Equation 3-11, substituting Equation 3-4 into the resulting expression, and then cancelling common terms, the following expression can be obtained:

$$\Delta V = e^T(l) \chi(l, x) + e^T(l) \Omega(l, x) - (c_1 + k_n + k_1) e^T(l) e(l). \quad (3-12)$$

By using Equation 3-7, the expression in Equation 3-12 can be upper bounded as

$$\begin{aligned}\Delta V &\leq c_1 \|e(l)\|^2 + c_2 \|e(l)\| - (c_1 + k_n + k_1) \|e(l)\|^2 \\ &\leq c_2 \|e(l)\| - k_n \|e(l)\|^2 - k_1 \|e(l)\|^2.\end{aligned}\tag{3-13}$$

Completing the squares on the first two terms in Equation 3-13 yields the following upper bound

$$\Delta V \leq -k_1 V(e, l) + \frac{c_2^2}{4k_n}.\tag{3-14}$$

Lemma 13.1 of [24] can now be invoked to conclude that

$$V(e, l) \leq b^l V(e(l_0), l_0) + \left(\frac{1 - b^l}{k_1}\right) \frac{c_2^2}{4k_n},\tag{3-15}$$

where

$$b = 1 - k_1,$$

where $0 < k_1 \leq 1$. Based on Equation 3-15, an upper bound for $e(l)$ can be developed as

$$\|e(l)\|^2 \leq b^l \|e(l_0)\|^2 + \left(\frac{1 - b^l}{k_1}\right) \frac{c_2^2}{4k_n}.\tag{3-16}$$

The ultimate bound in Equation 3-16 asymptotically converges as

$$\lim_{l \rightarrow \infty} \|e(l)\|^2 = \frac{c_2^2}{4k_1 k_n}.\tag{3-17}$$

From Equation 3-17, the ultimate bound can be decreased by increasing k_n ; however, the magnitude of k_n is restricted by Equation 3-9 and the constraint that $0 < P_i(l) \leq P_{\max}$.

3.3 Estimation of Error at Unsamped Instances

The developed controller operates at discrete times using a predefined sampling rate. The stability analysis in Section 3.2 only proves that the controller can achieve arbitrarily low error at the sampling times. In this section, an approximate analysis of the error is provided between the sampling times, and the mean-squared error is shown to be bounded by a constant that depends on the time between samples.

Consider the performance for large t , such that the error magnitude satisfies $|e(l)| = |x(l) - \gamma| < \varepsilon$. Let T_s denote the time between samples. Then the error for the signal from MT i at time t , where $lT_s < t < (l+1)T_s$ is

$$e_i(t) = x_i(t) - \gamma = \frac{g_{ii}(t)P_i(t)}{I_i^a(t)} - \gamma. \quad (3-18)$$

Letting $\Delta g_{ii}(t) = g_{ii}(t) - g_{ii}(lT_s)$ and using Equation 2-11, the error can be written as

$$\begin{aligned} e_i(t) &= \frac{a[g_{ii}(l) + \Delta g_{ii}(t)]P_i(t)}{\sum_{j \neq i} [g_{ij}(l) + \Delta g_{ij}(t)]P_j(l) + a\eta_i(t)} - \gamma \\ &= \frac{ag_{ii}(l)P_i(t) + a\Delta g_{ii}(t)P_i(t)}{\sum_{j \neq i} g_{ij}(l)P_j(l) + \sum_{j \neq i} \Delta g_{ij}(t)P_j(l) + a\eta_i(t)} - \gamma. \end{aligned} \quad (3-19)$$

To facilitate the analysis, under the assumption of a large number of mobile stations operating in the current cell, the weak law of large numbers can be invoked to approximate the second term in the denominator as

$$\sum_{j \neq i} \Delta g_{ij}(t)P_j(l) \approx \sum_{j \neq i} E[\Delta g_{ij}(t)] = 0. \quad (3-20)$$

Thus, the magnitude of the error can be approximated as

$$|e_i(t)| \approx \left| \frac{ag_{ii}(l)P_i(t) + a\Delta g_{ii}(t)P_i(t)}{\sum_{j \neq i} g_{ij}(l)P_j(l) + a\eta_i(t)} - \gamma \right|,$$

and upper bounded by

$$|e_i(t)| < \left| \frac{a\Delta g_{ii}(t)P_i(t)}{\sum_{j \neq i} g_{ij}(l)P_j(l) + a\eta_i(t)} \right| + \varepsilon_{CT}. \quad (3-21)$$

Noting that $E[\Delta g_{ii}(t)] = 0$, the mean-squared error at time t is bounded by

$$E[e_i^2(t)] < \frac{a^2 E[\Delta g_{ii}^2(t)] P_i^2(t)}{\left[\sum_{j \neq i} g_{ij}(l) P_j(l) + a\eta_i(t) \right]^2} + \varepsilon_{CT}^2, \quad (3-22)$$

where the expectation $E[\Delta g_{ii}^2(t)]$ is with respect to the random change in the fading $\Delta g_{ii}(t)$.

Let $R_g(\tau)$ be the autocorrelation function of the channel gain process. The expected value in Equation 3-22 can be written as

$$\begin{aligned} E[\Delta g_{ii}^2(t)] &= E \{ [g(t) - g(lT_s)]^2 \} \\ &= E[g^2(t)] - 2E[g(t)g(lT_s)] + E[g^2(lT_s)] \\ &= 2R_g(0) - 2R_G(\tau), \end{aligned} \quad (3-23)$$

where $\tau = t - lT_s$. In most systems, the sampling time will be fast enough that the exponential path loss and shadowing can be modeled as constant between sampling times, and thus the effects of multi-path fading is only considered. The autocorrelation function for the power in a Rayleigh fading process (refer to Figure 3-1) is given by [23]

$$R_g(\tau) = J_0^2(2\pi f_n \tau), \quad (3-24)$$

where J_0 is the zeroth-order Bessel function of the first kind, and f_n is the Doppler spread. The Doppler spread is given by fv/c , where f is the carrier frequency, v is the mobile velocity, and c is the speed of light.

Then, the mean-squared error is bounded by

$$\begin{aligned} E[e_i^2(t)] &< \frac{2a^2 [1 - J_0^2(2\pi f_n \tau)] P_i^2(t)}{\left[\sum_{j \neq i} g_{ij}(l) P_j(l) + \eta_i(t) \right]^2} + \varepsilon_{CT}^2 \\ &< 2a^2 [1 - J_0^2(2\pi f_n T_s)] \frac{P_{max}^2}{n^2 P_{min}^2} + \varepsilon_{CT}^2, \end{aligned} \quad (3-25)$$

where the weak law of large numbers is applied to the denominator with $E[g_{ij}^2(l)] = 1$. Here, P_{max} and P_{min} are, respectively, the maximum and minimum transmit powers allocated to a non-overfaded user. By taking into account the maximum power ratio P_{max}/P_{min} , number of users n , spreading gain a , and maximum MT velocity, T_s can be

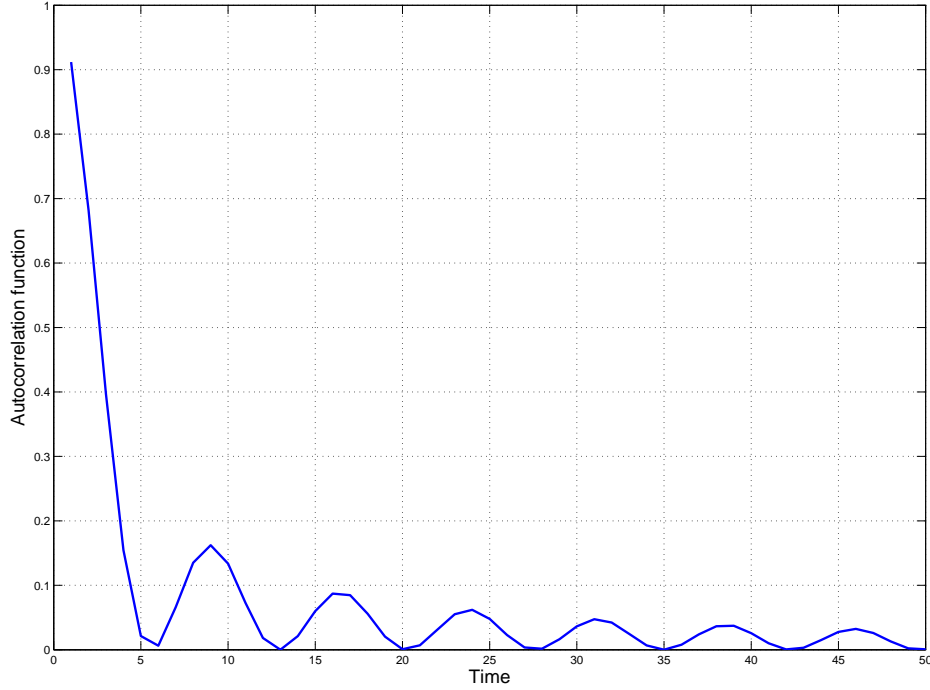


Figure 3-1. Autocorrelation function for fading.

selected to make the mean-square error be arbitrarily close to ε_{CT} . However, since the mean-square error can never be identically 1, it is not possible to obtain a zero error convergence result for this discrete-time system.

To give an idea of the implication of Equation 3–22, consider the error when $\varepsilon_{CT} \approx 0$. Let the carrier frequency $f = 900\text{MHz}$, and maximum velocity $v = 30\text{ miles/hour}$. Then the Doppler spread is 40.2Hz . To achieve a maximum mean-square error of 0.1SNR_{max} , where $\text{SNR}_{max} = \frac{2a^2 P_{max}^2}{n^2 P_{min}^2}$, the sampling time must be approximately 1.8ms . The ability to achieve this goal depends on the data rate in the system. For example, at 100kbps data rate, this requires a power control update every 178bits .

3.4 Simulation

3.4.1 Network Mobility Model

A cellular network topology was built in MATLAB, and the mobility of the MTs are modeled by a steady state (stationary) distribution model (i.e., [25], [26]). A

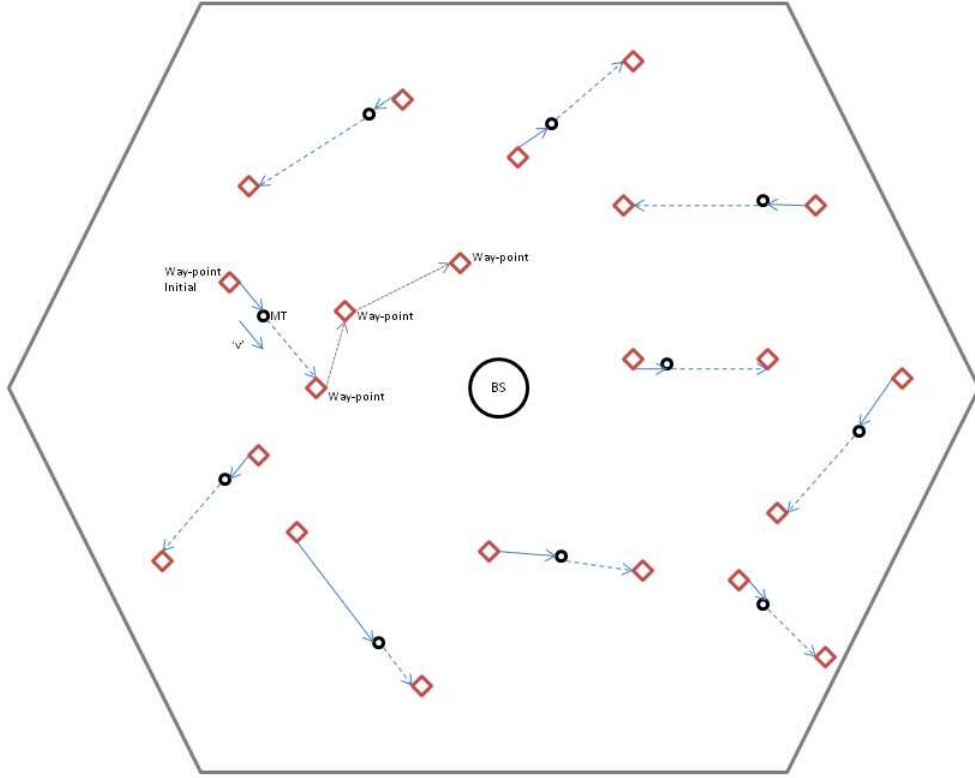


Figure 3-2. Cellular network topology - random way-point mobility model

Random-Waypoint model is used to simulate the mobility of the MTs. Figure 3-2 shows a typical cellular network topology built using a Random Way-Point model [26].

The error signal is expressed as

$$e_{i_{dB}}(l) = 10 \log \left(\frac{x_i(l)}{\gamma} \right) dB, \quad (3-26)$$

where $\gamma = 8dB$ is the target SINR as defined in Section 3.1.1 with a range between 6 and 10dB. Thermal noise, η , is set to $-110dBm$. A Rayleigh faded channel is created using the channel sampling time of 1.7ms obtained from the error analysis (Section 3.3) and the Doppler frequency, given in Equation 2-6, where $\lambda = 0.33m$ is the wavelength of the signal. The probability density function of the velocity is given by [26]

$$f_i(v) = \frac{C_h}{v} f_{V|h}^0(v), \quad (3-27)$$

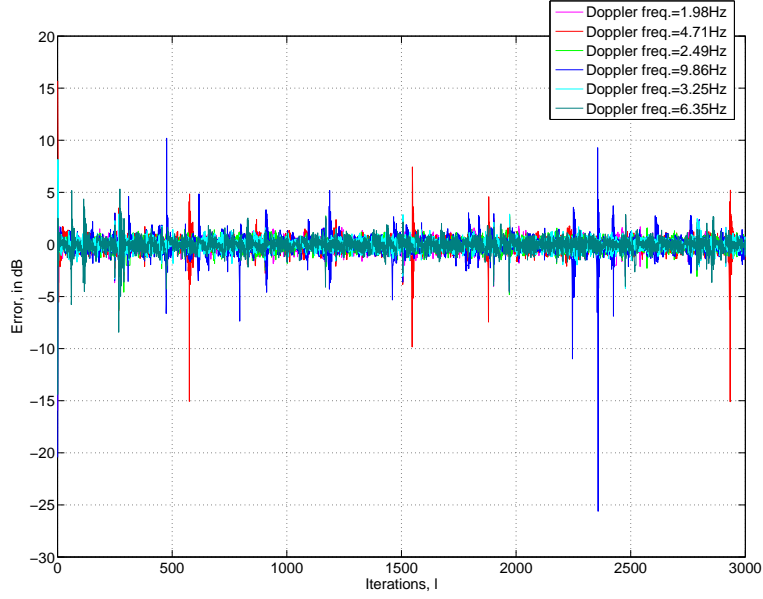


Figure 3-3. Error plot: MTs with low doppler frequencies.

where

$$\begin{aligned}
 f_{V|h}^0(v) &= \frac{1}{v_{\max} - v_{\min}} \\
 &= \frac{1}{48km/hr - 2km/hr} = \frac{1}{46km/hr}
 \end{aligned} \tag{3-28}$$

is a classical choice for the density of the velocity, and $C_h = 14.47$ is the normalizing constant. The subscript h is used to denote the phase of the MT [26]. The velocity for each of the MTs is obtained from Equation 3-27 using the inverse transform method as

$$v = \exp(3.179r + 0.6931), \tag{3-29}$$

where r is uniformly distributed between 0 and 1. The Doppler frequency is obtained from Equation 3-29 and by measuring θ periodically. Path loss, with free space propagation effects (near-field effects), and log-normal shadowing are modeled [19] as shown in Equation 2-1 and Equation 2-2.

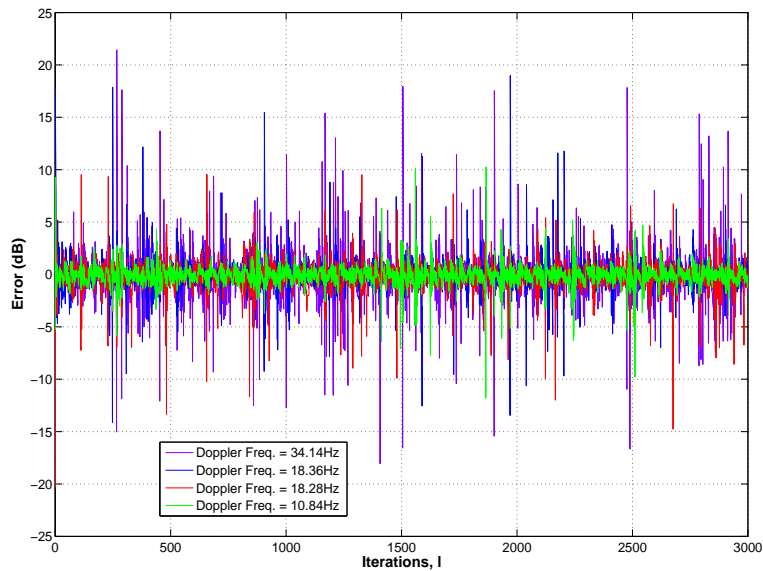


Figure 3-4. Error plot: MTs with high doppler frequencies.

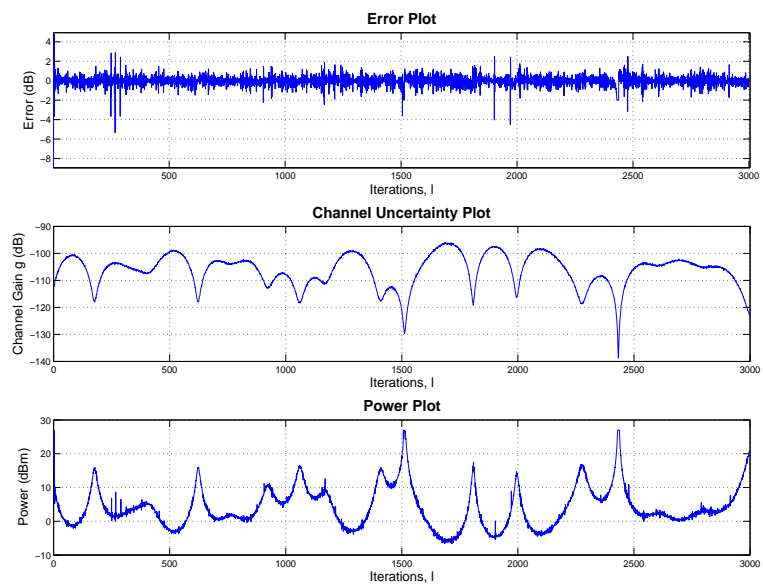


Figure 3-5. Error, channel gain and power plot: MT with a doppler frequency of 1.98 Hz.

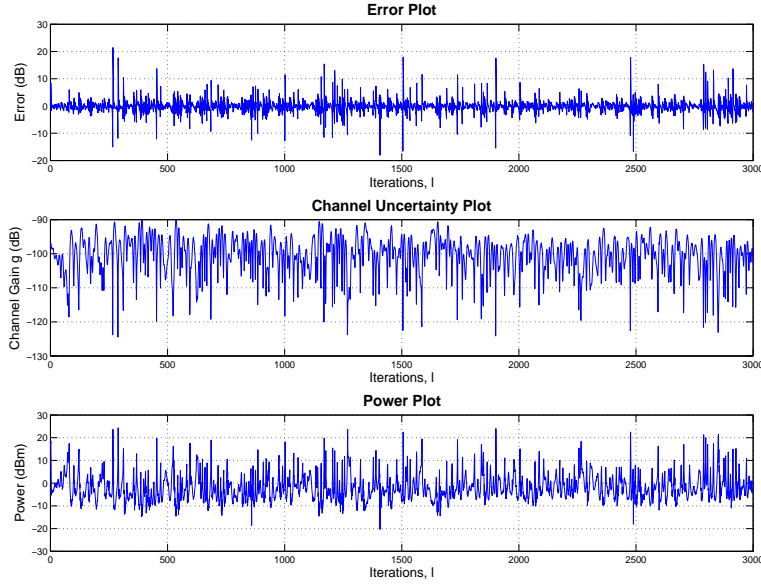


Figure 3-6. Error, channel gain and power plot: MT with a doppler frequency of 34.14 Hz.

3.4.2 Simulation Results

The results in Figures 3-3-3-6 are obtained with

$$c_1 = 8 \times 10^{-5}, \quad k_1 = 5 \times 10^{-5}, \quad k_n = 1.625,$$

and the spreading factor a is chosen as 320. Figures 3-3 and 3-4 depict the SINR errors for radio links operating at Doppler frequencies ranging from $0 - 10Hz$ and from $10 - 35Hz$, respectively. Figures 3-5 and 3-6 depict the SINR error, channel uncertainty, and power transmission levels for Doppler frequencies of $1.98Hz$ and $34.14Hz$, respectively. These plots indicate the intuitive notion that the SINR error is within the desired threshold for more samples at lower Doppler frequencies than at the higher frequencies. The second column of Table 3-1 quantifies the percentage of samples that lie within the desired SINR range for each Doppler frequency. When samples exceed the upper limit of the desired SINR range (i.e., $x_i(l) \geq \gamma_{\max}$), the QoS for the individual link is not compromised. However, exceeding the upper limit is undesirable because the interference to other links increases, potentially leading to an outage (i.e., when $x_i(l) \leq \gamma_{\min}$) [6–8]. An outage

Table 3-1. Percentage of samples within the desired SINR range

Doppler frequency (Hz)	% of samples where $\gamma_{\min} \leq x_i \leq \gamma_{\max}$	% of samples where $x_i \leq \gamma_{\min}$
1.98	98.97	0.23
2.49	98.67	0.27
3.25	99.23	0.40
4.71	97.47	1.23
6.35	97.63	0.83
9.86	94.90	1.97
10.84	95.07	2.47
18.28	88.33	3.87
18.36	88.86	5.13
34.41	75.40	10.30

of a link does compromise the quality of service in the sense that the signal may not be decoded at that particular sample. The third column of Table 3-1 quantifies the percentage of samples that experience an outage for each Doppler frequency, particularly due to fading [14, 15].

Figures 3-3 through 3-6 and Table 3-1 indicate that some samples fall outside of the desired SINR range (and experience an outage) with increasing occurrences at higher Doppler frequencies. The simulation model included a realistic upper limit on the available power (i.e., $27dBm$ ($500mW$)) with a fixed sampling frequency. The simulation also yields rapid changes in the channel gains (i.e., high frequency components in the uncertainty g_{ii}). These rapid changes are influenced by fading, which in turn deteriorates the performance of the controller, especially at higher Doppler frequencies (i.e., the upper bound c_2 in Equation 3-7 and Equation 3-17 has to be large to upper bound these effects). These rapid changes are exacerbated by MTs coming out of a deep faded zone (i.e., the channel gain is very close to zero) and the channel gain at the next sample can lead to high value causing interference to other users. Increasing k_n can counter these effects (i.e., see Equation 3-17), but the magnitude of k_n is limited by the power update law in Equation 3-9 and the constraint that $0 < P_i(l) \leq 500mW$. In some other cases this phenomena is

coupled with over-fading, when the power of some MTs reach an upper saturation limit and the controller can no longer increase the power to compensate for the fading.

CHAPTER 4
PREDICTION-BASED POWER CONTROL OF DISTRIBUTED CELLULAR
COMMUNICATION NETWORKS WITH TIME-VARYING CHANNEL
UNCERTAINTIES

Fast changing radio channels in a CDMA based cellular network have detrimental effects on the control efforts required to regulate the SINR to the desired level, especially for channels with high doppler frequency MTs. The motivation behind introducing a prediction-based power control algorithm is to meet the problems associated with rapid changes in the channel gain (by orders of magnitude between power update intervals) influenced by fading and exacerbated by the MTs coming out of the 'deep faded' zone. For a fast fading channel, a reliable prediction of the channel coefficient is required for accurate control design. For this purpose, a linear prediction filter is used in this chapter to estimate the channel fading parameter and this information is fed to the controller. A controller is developed in this chapter that uses local SINR measurements from the current and neighboring cells ([2], [1]) to maintain the SINRs of all the MTs present in the acceptable communication range. A Lyapunov based analysis is provided to explain the bound which the SINR error reaches, the size of which can be reduced by choosing appropriate control gains. The power control algorithm is simulated on a cellular network with distributed cells and the results indicate that the controller regulates the SINRs of all the MTs with low outage probability.

Due to the fast fading channel that a power controller has to encounter before ensuring acceptable communication between the MTs and the BS, prediction of the fading power would provide the controller with useful channel information. Earlier research conducted by Hallen on fading prediction focused on long range prediction [27–31] based on the fact that the amplitude, frequency and phase of each multi-path component vary much slower than the actual fading coefficient $X_i(\cdot)$. In [28], fading channel prediction is combined with transmitter signal optimization to mitigate the effects of deep fades. Physical channel modeling, with adaptive prediction was presented in [29]. Consequently,

focus was laid on performance analysis of long range prediction, transmitter diversity and adaptive long range prediction of fast fading channel coefficients [32].

In this chapter, the basic concepts on the radio channel characteristics as discussed above is analyzed and power of the fading coefficient is predicted, which is used in the subsequent control design. More specifically, for accurate prediction, more recent samples are used to estimate the fading coefficient at the next instance, unlike the long range fading prediction schemes where the goal is to predict the pattern of the fading envelope. For this purpose, a linear Minimum Mean Square Error (MMSE) predictor is used to obtain a reliable prediction of the fading coefficient at the next instance. Lyapunov based analysis is performed to provide an ultimate bound on the SINR error, the size of which can be reduced by choosing appropriate control gains. In addition, variations in other components of the radio channel such as path loss and log-normal shadowing are also accounted for using this analysis tool. Simulation results are provided for analysis and verification of results, and motivation is provided for future work.

4.1 Network Model

The SINR $x(l) \triangleq \left[x_1(l) \ x_2(l) \ \dots \ x_n(l) \right]^T \in \mathbb{R}^n$ is defined (in dB) for each radio link $i = 1, 2, \dots, n$ as

$$x_i(l) = 10 \log \left(\frac{a g_{ii}(l) P_i(l)}{I_i(l)} \right) \quad (4-1)$$

where the function $\log(\cdot)$ denotes the base 10 logarithm. The quantities inside the $\log(\cdot)$ function of Equation 4-1 is defined in Chapter 3.

Understanding how the SINR changes is beneficial for the development and analysis of the subsequent power control law. Taking the first difference of Equation 4-1 yields

$$\begin{aligned} \frac{\Delta x_i(l)}{T_s} &= \frac{x_i(l+1) - x_i(l)}{T_s} \\ &= \frac{[10 \log(g_{ii}(l+1)) - 10 \log(g_{ii}(l))]}{T_s} + \frac{u_i(l)}{T_s} \\ &\quad - \frac{[10 \log(I_i(l+1)) - 10 \log(I_i(l))]}{T_s}, \end{aligned} \quad (4-2)$$

where T_s is the power update interval, and $u(l) \triangleq \begin{bmatrix} u_1(l) & u_2(l) & \dots & u_n(l) \end{bmatrix}^T \in \mathbb{R}^n$ denotes an auxiliary control signal defined $\forall i = 1, 2, \dots, n$ as

$$u_i(l) = 10 [\log(P_i(l+1)) - \log(P_i(l))], \quad (4-3)$$

which is used to determine the power update law. The reason for defining the state as in Equation 4-1 is to obtain the controller as Equation 4-3 that would yield a power update that is more sensitive in operation than the power update Equation 3-9 used in Chapter 3.

After including measurement noise $\xi(l, x) \triangleq \begin{bmatrix} \xi_1(l, x_1) & \xi_2(l, x_2) & \dots & \xi_n(l, x_n) \end{bmatrix}^T \in \mathbb{R}^n$, the SINR at the next update interval $x(l+1) \triangleq \begin{bmatrix} x_1(l+1) & x_2(l+1) & \dots & x_n(l+1) \end{bmatrix}^T \in \mathbb{R}^n$ can be expressed as

$$x(l+1) = f_1(x(l)) + f_2(x(l)) + x(l) + u(l) + \xi(l, x), \quad (4-4)$$

where the channel gain functional $f_1(x(l)) \in \mathbb{R}^n$ is defined $\forall i = 1, 2, \dots, n$ as

$$f_1(x_i(l)) = 10 \log \left(\frac{g_{ii}(l+1)}{g_{ii}(l)} \right), \quad (4-5)$$

and the interference functional $f_2(x(l)) \in \mathbb{R}^n$ is defined $\forall i = 1, 2, \dots, n$ as

$$f_2(x_i(l)) = 10 \log \left(\frac{I_i(l)}{I_i(l+1)} \right). \quad (4-6)$$

4.2 Linear Prediction of Fading Coefficient

The development of a power controller for radio links in a CDMA network is challenging due to rapid, large scale changes in the coefficients of the nonlinear SINR dynamics. A further challenge is that the power capacity at each MT is constrained as

$$0 < P_i(l) \leq P_{\max},$$

where $P_{\max} \in \mathbb{R}$ is a maximum power level. As indicated in the simulation results in our previous effort [33], this dual problem leads to signal outages, especially when the MT

enters a deep faded zone. Motivated to address these issues, the current result estimates (or predicts) $|X_i(l+1)|^2$ and feeds this information to the controller to account for such fast changing channels and power limitations.

The prediction of $|X_i(l+1)|^2$ can be defined as a *Optimum Mean Square Error (MSE) problem* (see Appendix A), i.e.,

$$\begin{aligned} \varepsilon_{\min}^2 &= \min_{\hat{X}_i} E \left[\left(|X_i(l+1)|^2 - \hat{X}_i(l) \right)^2 \right] \\ &\text{given } |X_i(l)|^2, |X_i(l-1)|^2, \dots, |X_i(l-(n_1-1))|^2, \end{aligned}$$

where $\hat{X}_i(l)$ is the estimate of $|X_i(l+1)|^2$ that reduces the MSE. The optimum estimator is equal to the conditional mean [34]

$$E \left[|X_i(l+1)|^2 \mid |X_i(l)|^2, \dots, |X_i(l-(n_1-1))|^2 \right],$$

which is read as the expected value of $|X_i(l+1)|^2$ given $|X_i(l)|^2, \dots, |X_i(l-(n_1-1))|^2$.

Obtaining conditional estimate for nongaussian random processes (i.e., $|X_i(l+1)|^2$) is difficult; nonlinear estimates might be optimum for such cases and it requires higher order moments to obtain such nonlinear estimates. For these reasons, a linear estimator is chosen for predicting the fading variable $|X_i(l+1)|^2$.

The *Linear MMSE* for a non-gaussian random variable $|X_i(\cdot)|^2$ can be obtained from [34] as

$$\begin{aligned} \hat{X}_i(l) &= \sum_{m=l-(n_1-1)}^l \beta_i^{(m)} \left\{ |X_i(m)|^2 - \mu_{|X_i|^2} \right\} + \mu_{|X_i|^2} \\ &= \begin{cases} \sum_{m=l-(n_1-1)}^l \beta_i^{(m)} \left\{ |X_i(m)|^2 \right\} \\ + \mu_{|X_i|^2} \left(1 - \sum_{m=l-n_1}^l \beta_i^{(m)} \right); & f_n \neq 0 \\ |X_i(l)|^2; & f_n = 0 \end{cases} \quad (4-7) \end{aligned}$$

where $\mu_{|X_i|^2}$ is the mean of the random process $|X_i(\cdot)|^2$ for all l , f_n is the doppler frequency of the MT defined in Equation 2-6 at instance $\{(lT_p + 1) - (lT_p)\}$. The linear

estimate $\hat{X}_i(l)$ can take non-zero values if the prediction observation sampling rate (T_p) can be chosen appropriately. Based on [27], the sampling rate is chosen such that it is atleast the Nyquist rate, i.e., twice the maximum doppler frequency of the MT.

The $\beta_m^{(l-1)}$'s satisfy the orthogonality condition [see Appendix B]. Defining $\beta_i \triangleq [\beta_i^{(l-(n_1-1))} \quad \beta_i^{(l-(n_1-2))} \quad \dots \quad \beta_i^{(l)}]^T$ and using the orthogonality condition yields

$$\beta_i^T = \begin{bmatrix} E [|X_i(l+1)|^2 |X_i(l-(n_1-1))|^2] \\ E [|X_i(l+1)|^2 |X_i(l-(n_1-2))|^2] \\ \cdot \\ E [|X_i(l+1)|^2 |X_i(l)|^2] \end{bmatrix} Z^{-1}, \quad (4-8)$$

where $Z \in \mathbb{R}^{n_1 \times n_1}$ is defined $\forall j, k = 1, 2, \dots, n_1$ as

$$Z_{jk} = E [|X_i(l-(n_1-j))|^2 |X_i(l-(n_1-k))|^2].$$

The autocovariance function for $|X_i(\cdot)|^2$ is given by [23], [35]

$$\begin{aligned} R_{|X_i|^2}(lT_p) &= E [|X_i(l)|^2 |X_i(l+(lT_p))|^2] \\ &\approx J_0^2(2\pi f_n(lT_p)), \end{aligned} \quad (4-9)$$

(refer Figure 3-1) where J_0 is the zeroth-order Bessel function of the first kind. Therefore, from Equation 4-8,

$$\beta_i^T = \begin{bmatrix} J_0^2(2\pi f_n(T_p n_1)) \\ J_0^2(2\pi f_n(T_p(n_1-1))) \\ \cdot \\ J_0^2(2\pi f_n T_p) \end{bmatrix} Z^{-1}, \quad f_n \neq 0. \quad (4-10)$$

where the components of Z are defined $\forall j, k = 1, 2, \dots, n_1$ as

$$Z_{jk} = Z_{kj} = \begin{cases} J_0^2(2\pi f_n T_p |j-k|); & j \neq k \\ \sigma_{|X_i|^2}; & j = k \end{cases}, \quad f_n \neq 0. \quad (4-11)$$

By orthogonality, we have the LMMSE [34] as

$$\varepsilon_{\min}^2 = E \left[(|X_i(l+1)|^2)^2 \right] - \sum_{m=l-(n_1-1)}^l \beta_i^m E \left[|X_i(m)|^2 |X_i(l+1)|^2 \right].$$

Claim 4-1: The Linear predictor in Equation 4-7 is bounded based on the following facts. The power of the faded envelope $|X_i(\cdot)|^2$ at the receiver is bounded since in a radio link, the received power cannot be greater than the transmitted power (refer to Chapter 2 and Section 4.1). Therefore, the mean $\mu_{|X_i|^2}$ and the variance $\sigma_{|X_i|^2}$ are bounded. The coefficients of β_i in Equation 4-10 are bounded if the covariance matrix in Equation 4-11 is invertible. A prediction observation sampling rate (T_p) equal to or lower [31] than the power update rate (T_s) is chosen (such that it is atleast the Nyquist rate [27]) and the effect of additive noise is incorporated in Z [27], so that the inverse of Z can be computed.

Linear prediction of the fading process requires measurement of the $|X_1(\cdot)|^2$ at the current and previous instances; the performance of the predictor can be improved by increasing the number of measurements n_1 used to predict the fading process at instance $l+1$. Practically, as more measurements are used, the performance of the predictor does not improve but degrades due to computational problems associated with inverting the matrix Z . Note that the fading power of individual MTs at instance l used in the predictor is also used in the controller in the $\chi_X(l)$ term.

4.3 Control Development

4.3.1 Control Objective

The network quality of service can be quantified by the ability of the SINR to remain within a specified operating range with upper and lower limits, $\gamma_{\min}, \gamma_{\max} \in \mathbb{R}^n$ for each link defined $\forall i = 1, 2, \dots, n$ as

$$\gamma_{\min} \leq x_i(l) \leq \gamma_{\max}. \quad (4-12)$$

Keeping the SINR above the minimum threshold eliminates signal dropout, whereas remaining below the upper threshold minimizes interference to adjacent cells. As in Chapter 3, the control objective in this chapter is to regulate the SINR to a target value

for each channel, denoted by $\gamma \in \mathbb{R}^n$, while ensuring that the SINR remains between the specified lower and upper limits for each channel. To quantify this objective, a regulation error is defined as $e(l) \triangleq \begin{bmatrix} e_1(l) & e_2(l) & \dots & e_n(l) \end{bmatrix}^T \in \mathbb{R}^n$ where

$$e_i(l) = x_i(l) - \gamma, \quad \forall i = 1, 2, \dots, n. \quad (4-13)$$

4.3.2 Closed Loop Error System

By taking the first difference of Equation 4-13, and using Equation 2-1, Equation 4-4, and Equation 4-5, the open-loop error dynamics for each link can be determined as

$$\begin{aligned} \Delta e_i(l) = & 10 \log \left\{ g_{d_0} \left(\frac{d_i(l+1)}{d_0} \right)^{-\kappa} 10^{0.1\delta_i(l+1)} |X_i(l+1)|^2 \right\} \\ & - 10 \log \left\{ g_{d_0} \left(\frac{d_i(l)}{d_0} \right)^{-\kappa} 10^{0.1\delta_i(l)} |X_i(l)|^2 \right\} + f_2(x_i(l)) + \xi_i(l, x) + u_i(l). \end{aligned}$$

After using properties of the $\log(\cdot)$ function, the open-loop error dynamics can be simplified as

$$\begin{aligned} \Delta e(l) = & 10\chi_d(l, l+1) + \chi_\delta(l, l+1) + 10\chi_X(l+1) \\ & - 10\chi_X(l) + f_2(x(l)) + \xi(l, x) + u(l), \end{aligned} \quad (4-14)$$

where the auxiliary functions $\chi_d(l, l+1), \chi_\delta(l, l+1), \chi_X(\cdot) \in \mathbb{R}^n$ are defined $\forall i = 1, 2, \dots, n$ as

$$\chi_d(l, l+1) = \left[\kappa \log \left(\frac{d_1(l)}{d_1(l+1)} \right) \quad \kappa \log \left(\frac{d_2(l)}{d_2(l+1)} \right) \quad \dots \quad \kappa \log \left(\frac{d_n(l)}{d_n(l+1)} \right) \right]^T, \quad (4-15)$$

$$\chi_\delta(l, l+1) = [\delta_1(l+1) - \delta_1(l) \quad \delta_2(l+1) - \delta_2(l) \quad \dots \quad \delta_n(l+1) - \delta_n(l)]^T, \quad (4-16)$$

and

$$\chi_X(\cdot) = [\log |X_1(\cdot)|^2 \quad \log |X_2(\cdot)|^2 \quad \dots \quad \log |X_n(\cdot)|^2]^T. \quad (4-17)$$

Based on the model development in Chapter 2 (i.e., $d_i(\cdot)$ and $I_i(\cdot)$ are non-zero and bounded), the norm of $\chi_d(l, l+1)$ and $f_2(x(l))$ can be upper bounded by some positive

scalars as

$$\|\chi_d(l, l+1)\| \leq c_1, \quad (4-18)$$

and

$$\|f_2(x(l))\| \leq c_2. \quad (4-19)$$

Moreover, since $\delta(\cdot)$ is a zero-mean gaussian distributed variable (in dB) with a bounded standard deviation [19], then the norm of $\chi_\delta(l, l+1)$ can be upper bounded by some positive scalar as

$$\|\chi_\delta(l, l+1)\| \leq c_3, \quad (4-20)$$

and the measurement noise is assumed to be bounded, i.e.,

$$\|\xi(l, x)\| \leq c_4. \quad (4-21)$$

Based on Equation 4-14 and the subsequent stability analysis, the auxiliary power controller $u(l)$ is designed as

$$u(l) = -(k_n + k_p + k_e) e(l) - 10 \text{Log} \left(\left| \hat{X}(l) \right| \right) + 10 \chi_X(l), \quad (4-22)$$

where the notation $\text{Log} \left(\left| \hat{X}(l) \right| \right)$ is defined $\forall i = 1, 2, \dots, n$ as

$$\text{Log} \left(\left| \hat{X}(l) \right| \right) = \left[\log \left(\left| \hat{X}_1(l) \right| \right) \quad \log \left(\left| \hat{X}_2(l) \right| \right) \quad \dots \quad \log \left(\left| \hat{X}_n(l) \right| \right) \right]^T, \quad (4-23)$$

and

$$\left| \hat{X}_i(\cdot) \right| \neq 0, \quad (4-24)$$

where the components of $\text{Log} \left(\left| \hat{X}(l) \right| \right)$ are obtained from Equation 4-7, and the prediction sampling rate is chosen to be at least the Nyquist rate for Equation 4-24 to hold. From Equation 4-3, Equation 4-17, Equation 4-22, and Equation 4-23, the power update law for each radio channel is obtained as

$$P_i(l+1) = 10^{\Omega_i}, \quad \forall i = 1, 2, \dots, n, \quad (4-25)$$

where

$$\Omega_i = \frac{-(k_n + k_p + k_e) e_i(l)}{10} - \log \left(\left| \hat{X}_i(l) \right| \right) + \log |X_i(l)|^2 + \log(P_i(l)). \quad (4-26)$$

4.4 Stability Analysis

Theorem 4-1: The controller in Equation 4-22 and Equation 4-25 ensures that all closed loop signals are bounded, and that the SINR regulation error approaches an ultimate bound $\varepsilon(k_n, k_p, l_0) \in \mathbb{R}$ in the sense that

$$\|e(l)\| \rightarrow \varepsilon(k_n, k_p, l_0) \text{ as } l \rightarrow \infty \quad (4-27)$$

provided k_e in Equation 4-22 is selected as

$$0 < k_e \leq 1. \quad (4-28)$$

Proof: Let $V(e, l) : D \times [0, \infty) \rightarrow \mathbb{R}$ be a positive definite function defined as

$$V(e, l) = \frac{1}{2} e^T(l) e(l). \quad (4-29)$$

Taking the first difference of Equation 4-29, and substituting for Equation 4-14 yields

$$\begin{aligned} \Delta V &= e^T(l) [10\chi_d(l, l+1) + \chi_\delta(l, l+1) + 10\chi_X(l+1) \\ &\quad - 10\chi_X(l) + f_2(x(l)) + \xi(l, x) + u(l)]. \end{aligned} \quad (4-30)$$

Using Equations 4-18-4-21, and substituting Equation 4-22 into Equation 4-30 yields

$$\begin{aligned} \Delta V &\leq -k_e \|e(l)\|^2 + 10 \|e(l)\| \left(\left\| \chi_X(l+1) - \text{Log} \left(\left| \hat{X}(l) \right| \right) \right\| \right) - k_p \|e(l)\|^2 \\ &\quad + (10c_1 + c_2 + c_3 + c_4) \|e(l)\| - k_n \|e(l)\|^2. \end{aligned} \quad (4-31)$$

By completing the squares for the second and third lines, the inequality in Equation 4-31 can be further upper bounded as

$$\Delta V \leq -k_e \|e(l)\|^2 + \frac{25 \left(\left\| \chi_X(l+1) - \text{Log} \left(\left| \hat{X}(l) \right| \right) \right\| \right)^2}{k_p} + \frac{(10c_1 + c_2 + c_3 + c_4)^2}{4k_n}.$$

After using Equation 4-29, the following inequality can be developed

$$\Delta V \leq -k_e V + \frac{25 \left(\left\| \chi_X(l+1) - \text{Log} \left(\left| \hat{X}(l) \right| \right) \right\| \right)^2}{k_p} + \frac{(10c_1 + c_2 + c_3 + c_4)^2}{4k_n}. \quad (4-32)$$

Provided the sufficient condition in Equation 4-28 is satisfied, Lemma 13.1 of [24] can be invoked to conclude that

$$V(e, l) \leq (1 - k_e)^l V(e(l_0), l_0) + \left(\frac{1 - (1 - k_e)^l}{k_e} \right) \left[\frac{(10c_1 + c_2 + c_3 + c_4)^2}{4k_n} + \frac{25\varsigma}{k_p} \right], \quad (4-33)$$

where

$$\varsigma = \left\| \chi_X(l+1) - \text{Log} \left(\left| \hat{X}(l) \right| \right) \right\|^2$$

is upper bounded by a positive scalar c_5 , i.e.,

$$\varsigma \leq c_5$$

based on the results from Claim 4-1, the development in Chapter 2, and Section 4.2.

Based on Equation 4-33, an upper bound for the SINR error can be developed as

$$\|e(l)\|^2 \leq (1 - k_e)^l \|e(l_0)\|^2 + \left(\frac{1 - (1 - k_e)^l}{k_e} \right) \left[\frac{(10c_1 + c_2 + c_3 + c_4)^2}{4k_n} + \frac{25c_5}{k_p} \right]. \quad (4-34)$$

The assumption that $\chi_X(l) \in \mathcal{L}_\infty$, the fact that $\text{Log} \left(\left| \hat{X}(l) \right| \right) \in \mathcal{L}_\infty$ from Claim 4-1 and Equation 4-24, and the fact that $e(l) \in \mathcal{L}_\infty$ from Equation 4-34 can be used to conclude that $u(l) \in \mathcal{L}_\infty$ from Equation 4-22, and hence $P_i(l+1) \in \mathcal{L}_\infty$ from Equation 4-25. The ultimate bound in Equation 4-34 asymptotically converges as

$$\lim_{l \rightarrow \infty} \|e(l)\|^2 = \frac{(10c_1 + c_2 + c_3 + c_4)^2}{4k_n} + \frac{25c_5}{k_p}. \quad (4-35)$$

From Equation 4-35, the ultimate bound can be decreased by increasing k_n and k_p ; however, the magnitude of k_n is restricted by the constraint that $0 < P_i(l) \leq P_{\max}$.

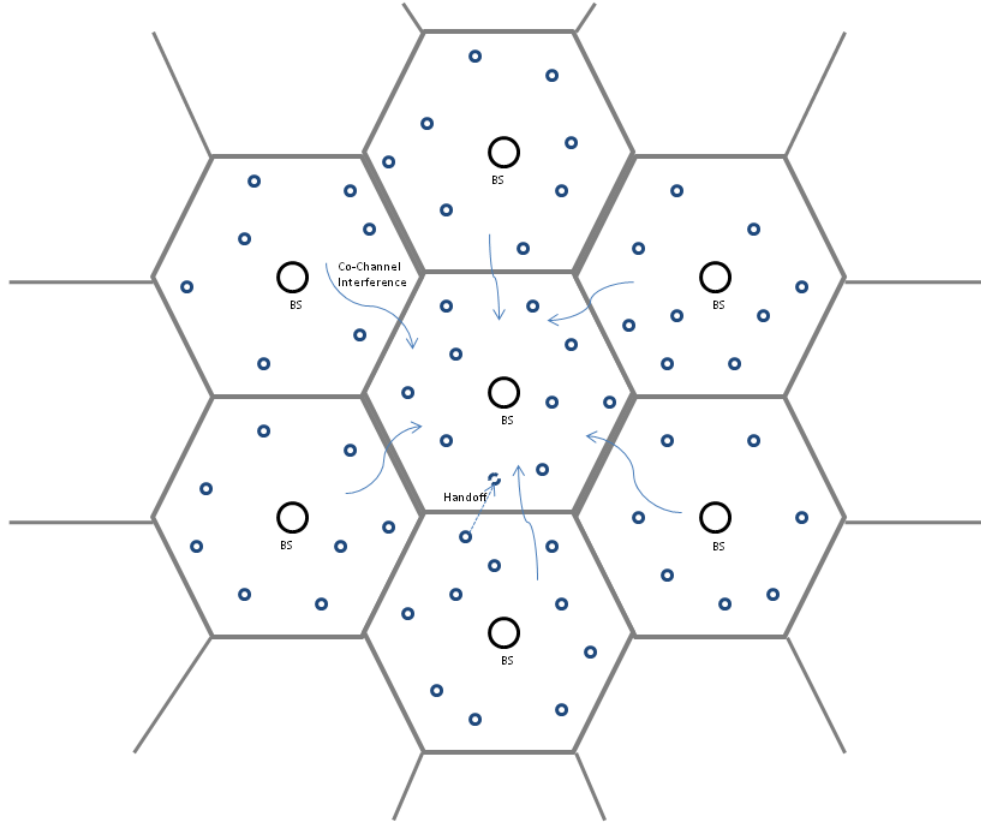


Figure 4-1. Distributed cellular network topology.

4.5 Simulation Results

A cellular network topology was built in MATLAB and the mobility of twenty MTs in the cell of interest is modeled by a steady state (stationary) distribution model (i.e., [25], [26]). A Random-Waypoint model is used to simulate the mobility of the MTs (refer to Section 3.4.1). The simulation is carried in a distributed cellular network with twenty MTs operating in the each of the six cells surrounding the cell of interest. Figure 4-1 shows a distributed cellular network topology.

The target SINR, γ is chosen as $8dB$ with a range between 6 and $10dB$, which is defined in Section 4.3.1. Thermal noise, η , is set to $-110dBm$. The initial power level for all the MTs is chosen as $10dBm$. A Rayleigh faded channel is created using the channel sampling time (T_s) of $1.7ms$, which is obtained by performing a continuous time SINR

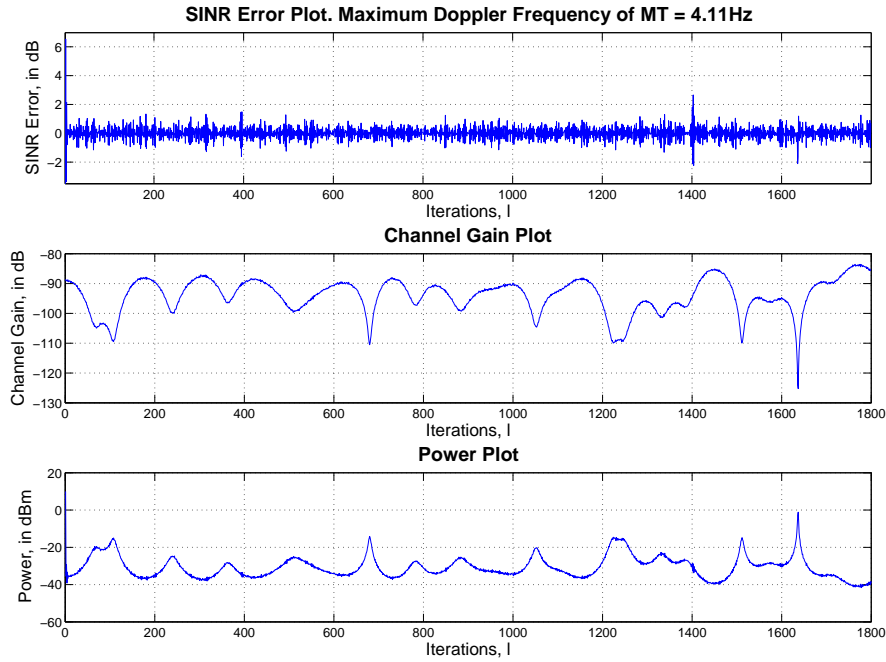


Figure 4-2. Error, channel gain, and power plot of a MT with maximum Doppler frequency 4.11 Hz.

error analysis (see Section 3.3), and the Doppler frequency Equation 2-6. The prediction observation sampling rate (T_p) is also chosen to be $1.7ms$. The velocity for each of the MTs is obtained from Equation 3-29. The angle θ is measured periodically and the Doppler frequency is obtained from Equation 3-29 and Equation 2-6, which is used to update the coefficients of the LMMSE predictor. Path loss, with free space propagation effects (near-field effects), and log-normal shadowing are modelled [19] as shown in Equation 2-1 and Equation 2-2.

The results in Figures 4-2 through 4-5 are obtained with

$$k_n = 0.00005, \quad k_p = 1.6, \quad k_e = 0.00008,$$

and the spreading factor a is chosen as 156. The number of samples used for prediction is 5. Figure 4-2 shows the SINR error, channel gain and power plots of a MT operating around a maximum doppler frequency of $4.11Hz$. The prediction error for this MT is

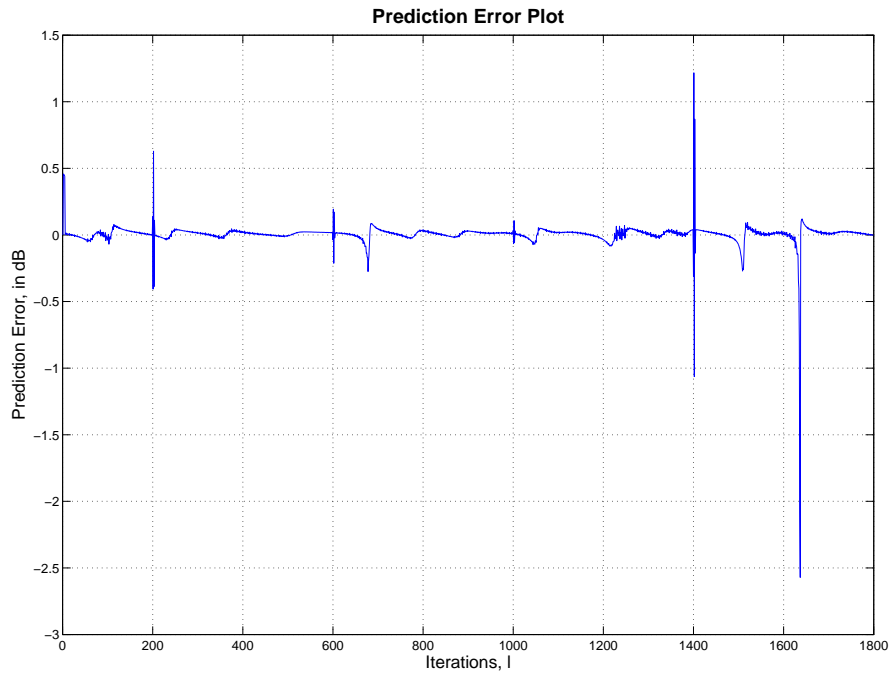


Figure 4-3. Prediction error of the MT with maximum Doppler frequency 4.11 Hz.

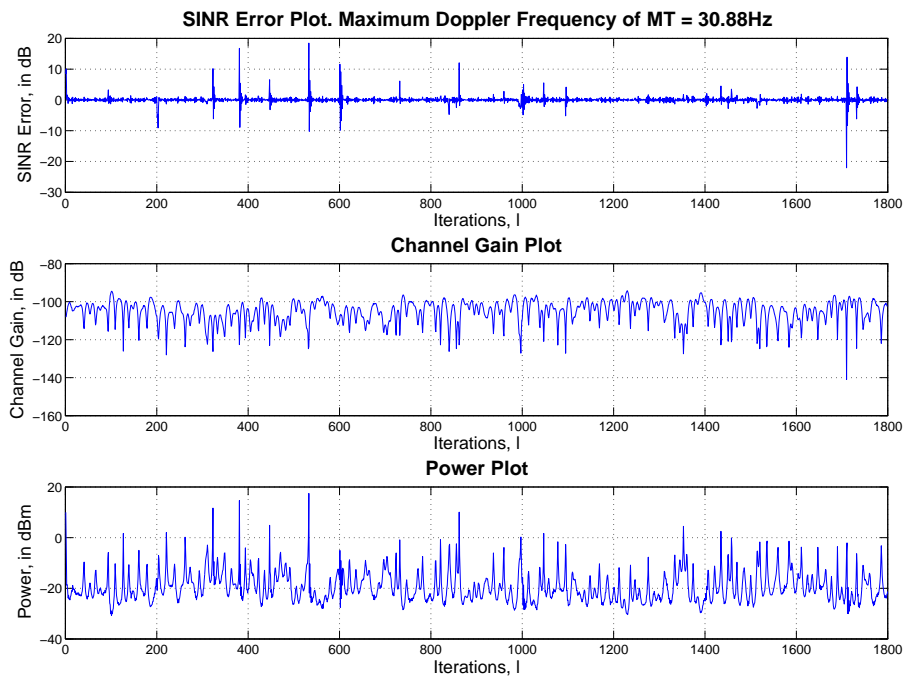


Figure 4-4. Error, channel gain, and power plot of a MT with maximum Doppler frequency 30.9 Hz.

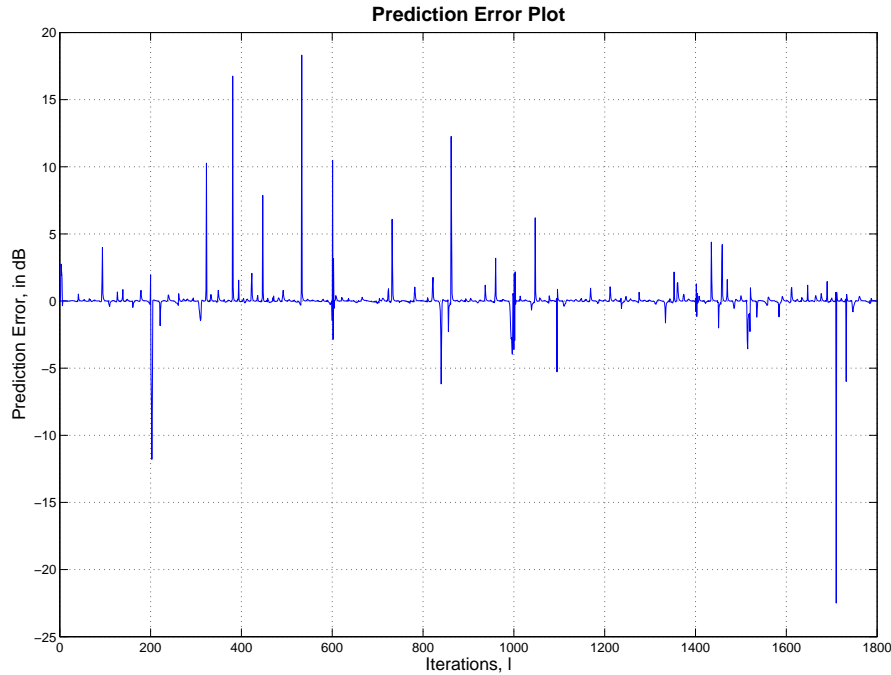


Figure 4-5. Prediction error of the MT with maximum Doppler frequency 30.9 Hz.

shown in Figure 4-3. It can be seen that the power controller regulates the SINR of the MT in the desired range almost perfectly. Figure 4-4 shows the SINR error, channel gain and power plots of a MT operating around a maximum doppler frequency of $30.88Hz$. The prediction error for this MT is shown in Figure 4-5. The inaccurate prediction of the linear predictor in the deep faded zones causes outage to the MT in those zones (Figures 4-4 and 4-5). The SINR of this radio link operating around a maximum doppler frequency of $30.88Hz$ is in the acceptable communication range at all other times, and the power required to achieve this is in the implementable range, well below the maximum power of $27dBm$ ($500mW$) of MTs.

Table 4-1 shows the statistics of the SINR error of all the MTs in the cell of importance. The second column of Table 4-1 quantifies the percentage of samples that lie within the desired SINR range for each Doppler frequency. When samples exceed the upper limit of the desired SINR range (i.e., $x_i(l) \geq \gamma_{\max}$), the quality of service for the

Table 4-1. Percentage of samples within the desired SINR range

Max. Doppler frequency (Hz)	% of samples where $\gamma_{\min} \leq x_i \leq \gamma_{\max}$	% of samples where $x_i \leq \gamma_{\min}$
0.80	99.78	0.05
1.78	99.84	0.05
2.32	99.78	0.05
3.96	99.67	0.05
4.00	99.56	0.16
4.11	99.50	0.27
4.17	99.78	0.05
6.19	99.45	0.27
6.82	99.73	0.16
6.88	98.72	0.72
7.46	99.39	0.22
8.07	98.78	0.61
10.61	99.45	0.22
11.25	99.33	0.22
11.52	99.00	0.55
14.61	98.61	0.83
23.03	98.50	0.83
26.29	98.17	0.94
26.50	95.89	2.17
30.88	96.33	1.94

individual link is not compromised. However, exceeding the upper limit is undesirable because the interference to other links increases, potentially leading to an outage (i.e., when $x_i(l) \leq \gamma_{\min}$) [6–8]. An outage of a link does compromise the quality of service in the sense that the signal may not be decoded at that particular sample. The third column of Table 4-1 quantifies the percentage of samples that experience an outage for each Doppler frequency, particularly due to fading [14, 15] and it can be inferred from this column that the outage ($x_i \leq \gamma_{\min}$) for all the MTs are regulated at below 3% at all times.

A new set of simulations were carried out for high-gain (centralized power control) [33] and prediction-based power control algorithms such that these algorithms are simulated on the same topology model with twenty MTs in a cell to obtain a clear implication of the result. Figure 4-6 shows the outage probability and maximum power requirement plots plotted against the maximum doppler frequency around which the

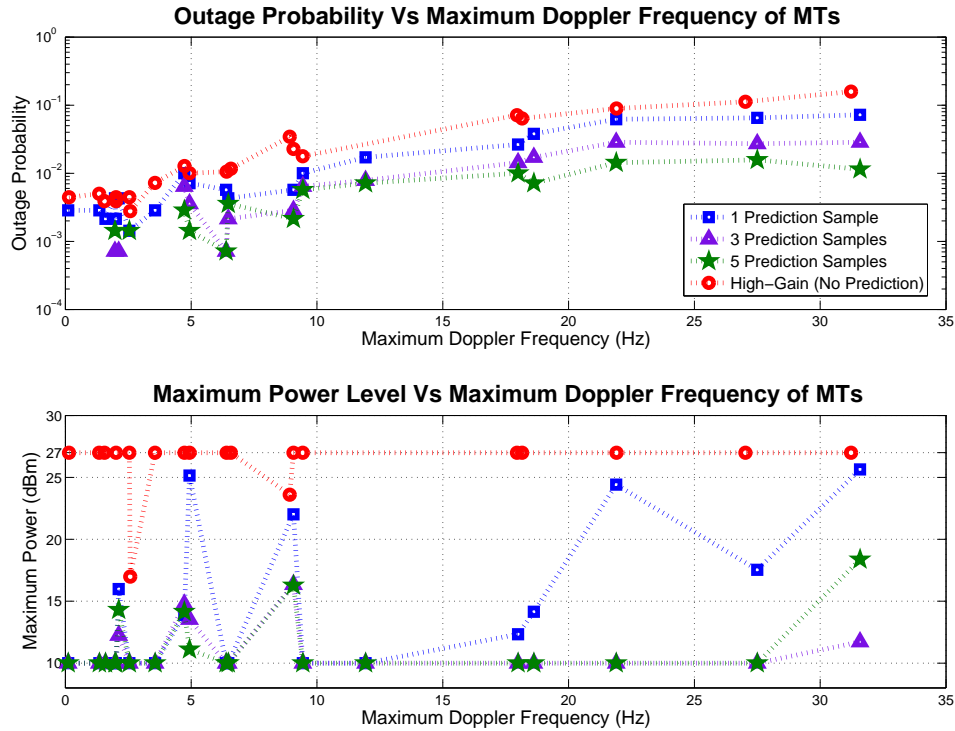


Figure 4-6. Comparison of high gain and predictive power control algorithms.

MTs operate for these power control algorithms. It can be seen that prediction-based power control algorithms are responsible for the radio link to operate with lower outage probabilities and much lower maximum power requirements when compared to MTs using high-gain power control algorithms. Also, note that most of the radio links that uses prediction-based power control algorithms require power lesser than the chosen initial power of 10dBm . It can also be inferred from Figure 4-6 that as the number of prediction observation samples n_1 increases, the performance of the power controller improves, i.e., radio links operate with lower outage probabilities.

CHAPTER 5 CONCLUSION

5.1 Summary of Results

Radio channel uncertainties, particularly fading, are responsible for the cellular network to be characterized as a nonlinear system. The fading process is characterized as a time-varying stochastic process which is responsible for significant power drops in certain regions known as deep faded regions causing problems in recovering the signal at the receiver. Further, restrictions in the maximum power at which the signals can be transmitted in such systems and bandwidth availability intensifies the need to develop power controllers for such radio links. To address these problems, controllers are designed that uses the Lyapunov-based tools to analyze the nonlinear system, and the simulation results are discussed to demonstrate and validate the theory behind the control design.

In Chapter 3, a robust power controller is developed for a wireless CDMA-based cellular network system. Lyapunov-based stability analysis is used to develop an ultimate bound for the sampled SINR error which can be decreased up to a point by increasing a nonlinear damping gain. An analysis is also provided to illustrate how mobility and the desired SINR regulation range affects the choice of channel update times. The choice of the update time also affects the ultimate bound that the sampled SINR error reaches - Lowering the sampling time reduces the ultimate bound. Simulations indicate that the SINRs of radio links operating with lower maximum Doppler frequency are maintained in the desired communication range. Radio links operating with a high maximum Doppler frequency have high outage probability due to the fastly time-varying nature of the channel uncertainties, and this motivated to use the concept of prediction to address the issue.

Chapter 4 introduces a MMSE prediction-based power control algorithm for a wireless CDMA-based distributed cellular networked system. A linear predictor is used to predict the fading power at the $l + 1$ th instant, and this information is fed to the controller from

which the power update law is obtained, which in this case is logarithmic in operation unlike the proportional controller developed in Chapter 3. A Lyapunov-based analysis is used to develop an ultimate bound for the sampled SINR error which can be decreased up to a point by increasing a nonlinear damping gains. Simulations indicate that the SINRs of all the radio links are regulated in the region $\gamma_{\min} \leq x_i(\cdot) \leq \gamma_{\max}$ with a outage probability of less than 3%. Local SINR measurements are used to simulate the distributed cellular network. Outages at some regions were determined to be due to limitations of the linear predictor, especially in the deep faded zones.

5.2 Recommendations for Future Work

In order to improve to performance of the controller designed in Chapter 4, more sophisticated prediction and control development concepts are required in such highly time-varying radio channels as encountered in the fading radio channels of urban environments. Wiener filters and other Lyapunov-based adaptive control development techniques can be used to improve the quality of service for cellular communication networks. Optimal control development for such nonlinear stochastic radio channels can potentially enhance the radio link quality of cellular communication networks.

The modeling and the control development methodologies followed in this work can be extended to wireless Mobile Ad-Hoc Networks (MANETs), where in addition to the random time-varying phenomena in the radio channel, unpredictable topological changes, bandwidth and power constraints, multiuser interference, time-delays (due to contention, back-off, etc), link scheduling and routing are some of the additional challenges encountered. Modeling and embedding such factors experienced in MANETs in the system model developed in this thesis for developing power control algorithms, and optimizing its performance based on the constraints in MANETs is potentially the next goal in this line of research.

APPENDIX A
ESTIMATION OF RANDOM PROCESSES

A-1 General MMSE based estimation theory

Let $W(l)$ be some random process that needs to be estimated. The problem of finding the estimates of the zero mean gaussian random variables can be defined as follows.

$$\begin{aligned}
 \varepsilon_{\min}^2 &= \min_{\hat{W}(l)} E \left[\left(W(l) - \hat{W}(l) \right)^2 \right] \text{ given } W(l-1), W(l-2), W(l-3), \dots \\
 &= \min_{\hat{W}(l)} E \left[\left(W^2(l) - 2\hat{W}(l)W(l) + \hat{W}^2(l) \right) \right] \text{ given } W(l-1), W(l-2), W(l-3), \dots \\
 &= \min_{\hat{W}(l)} E \left[W^2(l) \right] - 2\hat{W}(l)E \left[W(l) \right] + \hat{W}^2(l) \text{ given } W(l-1), W(l-2), W(l-3), \dots \quad (\text{A-1})
 \end{aligned}$$

To find the minimum value of the estimate of W ,

$$\begin{aligned}
 \frac{d}{d\hat{W}(l)} \left\{ E \left[W^2(l) \right] - 2\hat{W}(l)E \left[W(l) \right] \right\} &= 0 \text{ given } W(l-1), W(l-2), W(l-3), \dots \\
 \implies 0 - 2E \left[W(l) \right] + 2\hat{W}(l) &= 0 \text{ given } W(l-1), W(l-2), W(l-3), \dots
 \end{aligned}$$

The estimate is given by [34]

$$\hat{W}(l) = E \left[W(l) \mid W(l-1), W(l-2), W(l-3), \dots \right], \quad (\text{A-2})$$

The conditional estimate is given by

$$E \left[W(l) \mid W(l-1), W(l-2), W(l-3), \dots \right],$$

where $W(l), W(l-1), W(l-2), W(l-3), \dots$ are all jointly gaussian and $W(l-1), W(l-2), W(l-3), \dots$ are the past values of the random variable W that are used to estimate the current value $W(l)$.

A-2 Gaussian Case

The conditional probability density function is given by [36]

$$\begin{aligned} & f_{W(l)} [W(l) | W(l-1), W(l-2), W(l-3), \dots] \\ &= \frac{f_{W(l), W(l-1), W(l-2), \dots} [W(l), W(l-1), W(l-2), W(l-3), \dots]}{f_{W(l-1), W(l-2), \dots} [W(l-1), W(l-2), W(l-3), \dots]}, \end{aligned} \quad (\text{A-3})$$

where the numerator and denominator are joint density functions of the zero-mean gaussian random variables W upto instants l and $l-1$ respectively. The Covariance Matrices K_n and K_{n-1} are defined as follows

$$\begin{aligned} K_n &= E [Y_l \cdot Y_l^T], \\ \text{and } K_{n-1} &= E [Y_{l-1} \cdot Y_{l-1}^T], \end{aligned}$$

where

$$\begin{aligned} Y_l &= \begin{bmatrix} W(l-s) & W(l-(s-1)) & \dots & W(l) \end{bmatrix}^T, \\ \text{and } Y_{l-1} &= \begin{bmatrix} W(l-s) & W(l-(s-1)) & \dots & W(l-1) \end{bmatrix}^T. \end{aligned}$$

Since the means of the random variables W are zero at any l

$$\begin{aligned} & f_{W(l)} [W(l) | W(l-1), W(l-2), W(l-3), \dots] \\ &= \frac{\exp \left\{ -\frac{1}{2} Y_l^T K_n^{-1} Y_l \right\}}{(2\pi)^{\frac{n}{2}} |K_n|^{1/2}} \cdot \left\{ \frac{\exp \left\{ -\frac{1}{2} Y_{l-1}^T K_{n-1}^{-1} Y_{l-1} \right\}}{(2\pi)^{\frac{(n-1)}{2}} |K_{n-1}|^{1/2}} \right\}^{-1}. \end{aligned} \quad (\text{A-4})$$

Since $W(l)$ is a zero-mean gaussian random process, the MMSE estimate is a linear estimate, i.e., $E [W(l) | W(l-1), W(l-2), W(l-3), \dots]$ can be obtained by manipulating Equation A-4. For a simple case with only one given value, the linear MMSE estimation is

given by

$$\begin{aligned} E [W(l) | W(l-1)] &= \mu_{W(l)} + \rho_{W(l)W(l-1)} \left(\frac{\sigma_{W(l)}}{\sigma_{W(l-1)}} \right) (W(l-1) - \mu_{W(l-1)}) \\ &= \left[\rho_{W(l)W(l-1)} \left(\frac{\sigma_{W(l)}}{\sigma_{W(l-1)}} \right) \right] W(l-1), \end{aligned} \tag{A-5}$$

where $\rho_{W(l)W(l-1)}$ is the autocorrelation function, $\sigma_{W(l)}$ and $\sigma_{W(l-1)}$ are the variances.

APPENDIX B
ORTHOGONALITY CONDITION

Let $Y, X_1, X_2, X_3, \dots, X_N$ be gaussian random variables with zero means. The MMSE estimate is the conditional mean, given by

$$E[Y | X_1, X_2, X_3, \dots, X_N] = \sum_{k=1}^N a_k X_k. \quad (\text{B-1})$$

The random variables $\left(Y - \sum_{k=1}^N a_k X_k\right), X_1, X_2, X_3, \dots, X_N$ are jointly gaussian. Since the first term is uncorrelated with all the rest, it can be inferred that the random variable $\left(Y - \sum_{k=1}^N a_k X_k\right)$ is uncorrelated with $X_1, X_2, X_3, \dots, X_N$. Therefore,

$$\begin{aligned} E \left[\left(Y - \sum_{k=1}^N a_k X_k \right) | X_1, X_2, X_3, \dots, X_N \right] &= E \left[\left(Y - \sum_{k=1}^N a_k X_k \right) \right] \\ &= E[Y] - \sum_{k=1}^N a_k E[X_k] = 0, \end{aligned}$$

since $E[Y] = E[X_k] = 0$. The condition

$$E \left[\left(Y - \sum_{k=1}^N a_k X_k \right) | X_1, X_2, X_3, \dots, X_N \right] = 0 \quad (\text{B-2})$$

is known as the *Orthogonality Condition*, which can also be written as

$$[Y - a^T X] \perp X, \quad (\text{B-3})$$

where

$$X = \begin{bmatrix} X_1 & X_2 & \dots & X_N \end{bmatrix}^T.$$

The a_i 's can be obtained from the orthogonality condition.

Note: From Equation [B-2](#), we get

$$E[Y | X_1, X_2, X_3, \dots, X_N] - \sum_{k=1}^N a_k E[X_k | X] = 0.$$

$$\begin{aligned}
&\implies E[Y | X_1, X_2, X_3, \dots, X_N] - \sum_{k=1}^N a_k X_k = 0 \\
&\implies E[Y | X_1, X_2, X_3, \dots, X_N] = \sum_{k=1}^N a_k X_k.
\end{aligned} \tag{B-4}$$

Thus, the conditional mean of a zero-mean gaussian random variable Y is given by a linear estimate of the given variables X_i s.

Calculation of a_i 's.

From the Orthogonality condition in Equation B-2, we get [34]

$$\begin{aligned}
E \left[\left(Y - \sum_{k=1}^N a_k X_k \right) | X_p \right] &= 0, \quad 1 \leq p \leq N \\
\implies E[Y X_p] &= \sum_{k=1}^N a_k E[X_k X_p], \quad 1 \leq p \leq N. \\
&\implies k_{YX} = a^T K_{XX},
\end{aligned} \tag{B-5}$$

where

$$\begin{aligned}
a &\triangleq \begin{bmatrix} a_1 & a_2 & \dots & a_N \end{bmatrix}^T, \\
k_{YX} &\triangleq \begin{bmatrix} E[Y X_1] & E[Y X_2] & E[Y X_3] & \dots & E[Y X_N] \\ K_{YX_1} & K_{YX_2} & K_{YX_3} & \dots & K_{YX_N} \end{bmatrix},
\end{aligned}$$

and the covariance matrix

$$K_{XX} = E[XX^T]. \tag{B-6}$$

From Equation B-5, we get

$$a^T = k_{YX} K_{XX}^{-1}. \tag{B-7}$$

REFERENCES

- [1] N. Bambos, S. Chen, and G. Pottie, "Channel access algorithms with active link protection for wireless communication networks with power control," *IEEE/ACM Trans. Networking*, no. 5, pp. 583–597, 2000.
- [2] G. Foschini and Z. Miljanic, "A simple distributed autonomous power control algorithm and its convergence," *IEEE Tran. Veh. Technol.*, vol. 42, pp. 641–646, 1993.
- [3] S. Grandhi and J. Zander, "Constrained power control in cellular radio systems," in *Vehicular Technology Conference, 1994 IEEE 44th*, 8-10 June 1994, pp. 824–828vol.2.
- [4] R. Jantti and S. Kim, "Second-order power control with asymptotically fast convergence," *IEEE J. Select. Commun*, vol. 18, no. 3, 2000.
- [5] R. D. Yates, "A framework for uplink power control in cellular radio systems," *IEEE J. Select. Areas Commun.*, vol. 13, pp. 1341–1347, Sept. 1995.
- [6] J. Zander, "Optimum global transmitter power control in cellular radio systems," in *IEEE Int. Symp. on Personal, Indoor and Mobile Radio Commun., London, U.K.*, 1991.
- [7] —, "Distributed cochannel interference control in cellular radio systems," *IEEE Tran. Veh. Technol.*, vol. 41, pp. 305–311, 1992.
- [8] —, "Performance of optimum transmitter power control in cellular radio systems," *IEEE Trans. Veh. Technol.*, vol. 41, pp. 57–62, 1992.
- [9] J. Aein, "Power balancing in systems employing frequency reuse," *COMSAT Tech. Rev.*, pp. 277–299, 1973.
- [10] H. Alavi and R. Nettleton, "Downstream power control for a spread spectrum cellular mobile radio system," in *Proc. IEEE GLOBECOM*, 1982, pp. 84–88.
- [11] S. Grandhi, R. Vijayan, and J. Zander, "Centralized power control in cellular radio systems," *IEEE Transactions on Vehicular Technology*, vol. 42, no. 4, November 1993.
- [12] R. D. Yates and C. Y. Huang, "Integrated power control and base station assignment," *IEEE Trans. Veh. Technol.*, vol. 44, pp. 638–644, Aug. 1995.
- [13] S. Dontula and S. Jagannathan, "Active link protection for wireless peer-to-peer and cellular networks with power control," in *World Wireless Congress*, 2004, pp. 612–617.
- [14] S. Kandukuri and S. Boyd, "Optimal power control in interference-limited fading wireless channels with outage-probability specifications," *IEEE Transactions on Wireless Communications*, vol. 1, no. 1, pp. 46–55, January 2002.
- [15] J. Papandriopoulos, J. Evans, and S. Dey, "Optimal power control for Rayleigh-faded multiuser systems with outage constraints," *IEEE Transactions on Wireless Communications*, vol. 4, no. 6, pp. 2705–2715, November 2005.

- [16] S. Jagannathan, *Wireless Ad Hoc and Sensor Networks*, F. L. Lewis, Ed. CRC Press, 2007.
- [17] S. Jagannathan, M. Zawodniok, and Q. Shang, “Distributed power control for cellular networks in the presence of channel uncertainties,” *IEEE Transactions on Wireless Communications*, vol. 5, no. 3, 2006.
- [18] R. Canchi and Y. Akaiwa, “Performance of adaptive transmit power control in $\pi/4$ DQPSK mobile radio systems in flat Rayleigh fading channels,” in *Vehicular Technology Conference, 1999 IEEE 49th*, vol. 2, 16-20 May 1999, pp. 1261–1265vol.2.
- [19] T. Rappaport, *Wireless Communications, Principles and Practice*. Prentice Hall, 1999.
- [20] L. Gao and T. Wong, “Power control and spreading sequence allocation in a cdma forward link,” *IEEE Trans. Inform. Theory*, vol. 50, no. 1, pp. 105–124, Jan. 2004.
- [21] N. Bambos, “Towards power-sensitive network architectures in wireless communications: Concepts, issues and design aspects,” *IEEE Pers. Commun.*, pp. 50–59, 1998.
- [22] A. J. Viterbi, *CDMA: Principles of Spread Spectrum Communication*. Addison Wesley, 1995.
- [23] R. H. Clarke, “A statistical theory of mobile-radio reception,” *Bell Syst. Technical J.*, vol. 47, no. 6, pp. 957–1000, Jul.–Aug. 1968.
- [24] J. Spooner, M. Maggiore, R. Ordonez, and K. Passino, *Stable Adaptive Control and Estimation for Nonlinear Systems*. Wiley, 2002.
- [25] S. PalChaudhuri, J.-Y. Le Boudec, and M. Vojnovic, “Perfect simulations for random trip mobility models,” in *Simulation Symposium, 2005. Proceedings. 38th Annual*, 4-6 April 2005, pp. 72–79.
- [26] J.-Y. Le Boudec and M. Vojnovic, “Perfect simulation and stationarity of a class of mobility models,” in *INFOCOM 2005. 24th Annual Joint Conference of the IEEE Computer and Communications Societies. Proceedings IEEE*, vol. 4, 13-17 March 2005, pp. 2743–2754vol.4.
- [27] A. Duel-Hallen, S. Hu, and H. Hallen, “Long range prediction of fading signals: Enabling adaptive transmission for mobile radio channels,” *IEEE Signal Processing Mag.*, vol. 17, no. 3, pp. 62–75, May 2000.
- [28] T. Eyceoz, A. Duel-Hallen, and H. Hallen, “Deterministic channel modeling and long range prediction of fast fading mobile radio channels,” *IEEE Commun. Lett.*, vol. 2, no. 9, pp. 254–256, Sept. 1998.

- [29] T. Eyceoz, S. Hu, and A. Duel-Hallen, "Performance analysis of long range prediction for fast fading channels," in *Proc. of 33rd Annual Conf. on Inform. Sciences and Systems CISS99*, vol. II, Mar. 1999, pp. 656 – 661.
- [30] S. Hu, H. Hallen, and A. Duel-Hallen, "Physical channel modeling, adaptive prediction and transmitter diversity for flat fading mobile channel," in *Signal Processing Advances in Wireless Communications, 1999. SPAWC '99. 1999 2nd IEEE Workshop on*, 9-12 May 1999, pp. 387–390.
- [31] S. Hu, T. Eyceoz, A. Duel-Hallen, and H. Hallen, "Transmitter antenna diversity and adaptive signaling using long range prediction for fast fading DS/CDMA mobile radio channels," in *Wireless Communications and Networking Conference, 1999. WCNC. 1999 IEEE*, 21-24 Sept. 1999, pp. 824–828vol.2.
- [32] T. Eyceoz, S. Hu, A. Duel-Hallen, and H. Hallen, "Adaptive prediction, tracking and power adjustment for frequency non-selective fast fading channels," in *Communication Theory Mini-Conference, 1999*, 6-10 June 1999, pp. 1–5.
- [33] S. Subramanian, J. M. Shea, and W. E. Dixon, "Power control of cellular communications with channel uncertainties," in *American Control Conference, 2009. ACC '09*, 2009, to appear.
- [34] H. Stark and J. W. Woods, *Probability and Random Processes with Applications to Signal Processing*, 3rd ed. Pearson Education, 2002.
- [35] W. C. Jakes, *Microwave Mobile Communications*. Wiley, 1974.
- [36] A. Leon-Garcia, *Probability and Random Processes for Electrical Engineering*, 2nd ed. Addison Wesley, 1994.

BIOGRAPHICAL SKETCH

Sankrith Subramanian was born in Chennai, India in 1985. He received his bachelor's degree in instrumentation and control engineering from St. Joseph's College of Engineering (Anna University), Chennai, India in May 2006. He received his Master of Science degree from the University of Florida in 2009. His interests lie in the field of networked control systems, nonlinear controls, wireless communication, signal processing and automation.

Sankrith pursued his Master of Science degree in the Department of Electrical and Computer Engineering and was a graduate research assistant in the Nonlinear Controls and Robotics group in the Department of Mechanical and Aerospace Engineering at the University of Florida, under the supervision of Dr. Warren E. Dixon. He was co-advised by Dr. John M. Shea of the Wireless Information Networking Group in the Department of Electrical and Computer Engineering at the University of Florida.

The primary focus of his research was to analyze wireless CDMA-based cellular communication networks with time-varying stochastic channel uncertainties and design Lyapunov-based nonlinear power controllers. Simulation demonstrations were provided with the help of realistic network topology models. His future interest is to extend and apply his research to wireless ad-hoc networks.